SYNTHESIS AND APPLICATION OF

MELAMINE-BASED DENDRIMER/SBA-15 HYBRID MATERIALS

A Thesis

by

JONATHAN DAVID LUNN

Submitted to the Office of Graduate Studies of
Texas A&M University
in partial fulfillment of the requirements for the degree of

MASTER OF SCIENCE

May 2006

Major Subject: Chemical Engineering

SYNTHESIS AND APPLICATION OF

MELAMINE-BASED DENDRIMER/SBA-15 HYBRID MATERIALS

A Thesis

by

JONATHAN DAVID LUNN

Submitted to the Office of Graduate Studies of
Texas A&M University
in partial fulfillment of the requirements for the degree of

MASTER OF SCIENCE

Approved by:

Chair of Committee,	Daniel F. Shantz
Committee Members,	David M. Ford
	Eric E. Simanek
Head of Department,	Kenneth R. Hall

May 2006

Major Subject: Chemical Engineering

ABSTRACT

Synthesis and Application of Melamine-based Dendrimer/SBA-15 Hybrid Materials.

(May 2006)

Jonathan David Lunn, B.S., Texas A&M University

Chair of Advisory Committee: Dr. Daniel F. Shantz

Porous inorganic materials that can be used in applications such as catalysis and separations have been intensely studied due to their potential stability, ease of recovery and high surface areas. Organic-inorganic hybrid materials meet these criteria by exploiting the physical robustness of porous inorganic materials and the chemical functionality of organic materials. While amorphous oxides are widely used industrially as inorganic supports, disordered pore structures make them difficult to characterize. Ordered-mesoporous-silica (OMS), such as SBA-15, that have ordered pores structures simplify characterization and are useful models for studying hybrid materials. Dendrimers, once appropriately functionalized, have high densities of uniformly distributed functional groups.

In this thesis, melamine-based dendrimer/SBA-15 hybrids were synthesized and characterized using a wide range of analytical techniques. This thesis shows that the porosity can be independently altered by varying 1) the dendrimer generation, 2) the linker molecule, and 3) the surface amine loading. Cu(II) sequestration results demonstrate that the peripheral functional groups of the dendrimer are readily accessible for binding.

This thesis also describes preliminary work toward preparing an enantioselective catalyst using L-proline supported on OMS. This work includes the synthesis and testing of three dendrimer-like proline derivatives. Future work in this area is outlined and will include synthesizing catalysts based on the dendrimer hybrid system previously described. Solution dendrimer syntheses will also be performed to create solution-based catalysts.

ACKNOWLEDGEMENTS

I would like to thank Dr. Daniel F. Shantz for his support and guidance over the past two years that I have been a graduate student in his research group. He has been a great teacher and mentor and I look forward to continuing work with him as a PhD student.

I thank my committee members, Dr. Eric Simanek and Dr. David Ford, for their time, effort and faith they have placed in me.

I also appreciate my colleagues in both the Shantz and Simanek research groups for their help, advice, scrutiny and interesting discussions. I specifically thank John Yoo, Dr. Sergio Gonzalez and Jenny Ristich for their work on the research covered in Chapter III, and Dr. Shane Carr for his TEM work. Also, thanks to Dr. Robert Sherman and Dr. Emily Hollink for their enormously valuable organic synthesis advice.

I thank my family and friends for their support. And finally, I thank God for providing me with the ability, will, and opportunity to complete this degree.

TABLE OF CONTENTS

Page

Page

LIST OF FIGURES

FIGURE Page

LIST OF TABLES

CHAPTER I

INTRODUCTION

1.1 Overview

Porous inorganic materials that can be used in applications such as catalysis and separations have been intensely studied over the last 50 years due to their potential stability, ease of recovery and high surface areas. These materials can be divided into three categories according to pore size: microporous (< 2nm), mesoporous (2-50nm), and macroporous (> 50nm).[1] It should be noted, however, that materials do not always belong exclusively to one category and may have a broad range of pore sizes or shapes.

Amorphous oxides, while widely used industrially, are complex due to their inherent disorder. From a fundamental viewpoint inorganic solids which are crystalline, or at least ordered, should be easier to understand. With this in mind, zeolites have received considerable interest in the later half of the last century. Zeolites, an example of a microporous material, are crystalline aluminosilicates with uniform micropores resulting from their crystal structure. Zeolites have shown to be very useful in applications such as ion-exchange, separations by size exclusion and catalytic cracking.[2] However, their use is limited by their small pore size which is usually less than 2nm.

Macroporous materials, on the other hand, can be easily modified; however, they have low surface areas. Mesoporous materials represent a good compromise between the high structural uniformity of zeolites and easily modified macroporous surfaces and thus hold the potential for a much larger range of effective chemical functions than micro- or

---

This thesis follows the style of *Chemistry of Materials*.

macro- porous materials. This is why the development of ordered mesoporous materials in the early 1990's was met with excitement and enthusiasm.

1.2 Ordered Mesoporous Silica

Ordered mesoporous silica (OMS) is a category of siliceous materials which, though they have been found not to be crystalline like zeolites, contain periodically arranged mesopores.[3-9] They can contain hexagonal, cubic or other pore topologies. Though many of these materials have only mesopores, some also contain micropores that are not necessarily ordered.[6,7] What distinguishes OMS from other siliceous materials is the long-range ordering of the mesopores. The synthesis of these materials is similar to that of zeolites and involves preparing a synthesis mixture of a tetraethoxysilane (or some other silica source), an organic structure-directing agent, and either an acid or base. The mixture is heated for an extended period of time, then filtered and washed. To remove the organic structure-directing agent, the resulting powder is either calcined at a high temperature or extracted.[3-9]

1.2.1 M41S

The first types of OMS were developed by the Mobil Corporation in the early 1990's and are commonly referred to as M41S (though not all of these materials are in fact ordered).[4,5] The most well-known and widely studied of this OMS type is MCM-41. MCM-41 has hexagonally arranged cylindrical pores which can vary from 2.5-10 nm in diameter depending on the template used. It is formed under basic conditions using surfactants as the structure directing agent, which is usually cetyltrimethylammonium

bromide (CTAB). Using CTAB, a typical pore size for MCM-41 is 4nm. Another M41S material, MCM-48, is cubic and its pore network can be represented by the *Ia3d* space group [3]. Figure 1.1 compares the TEM images of MCM-41 and MCM-48.

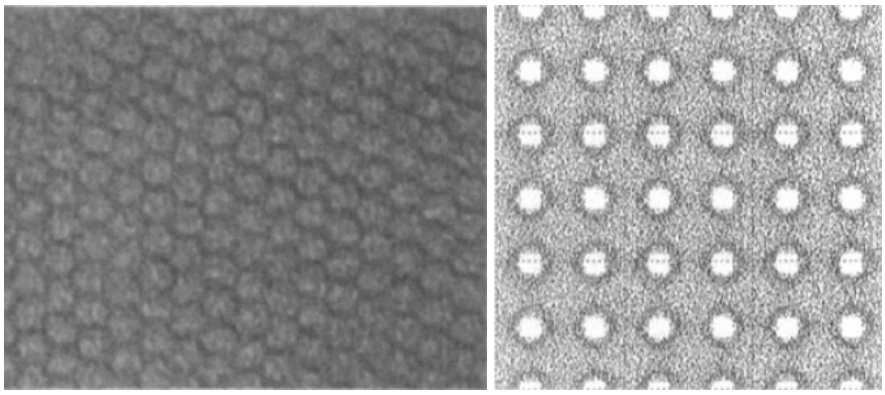

Figure 1.1 TEM images of (a) MCM-41[4], (b) MCM-48.[3]

1.2.2 SBA-15

SBA-15 is another ordered-mesoporous silica. It is one of a series of mesoporous materials developed in the mid-late 1990's by Stucky *et al.* at the University of California at Santa Barbara.[6,7] It has a hexagonal pore network (See Figure 1.2), like MCM-41, with accessible pore diameters in the range of 6-20 nm.[7] A typical pore size for SBA-15 is 8nm. SBA-15 is synthesized under acidic conditions using a triblock copolymer, Pluronic P123, as a structure-directing agent. Pluronic P123 is made up of two blocks of twenty hydrophilic ethylene oxide (EO) units separated by one block of seventy hydrophobic propylene oxide (PO) units ($EO_{20}PO_{70}EO_{20}$). Just as MCM-41 has a cubically ordered counterpart (MCM-48), SBA-15 has a cubic counterpart designated SBA-16 whose pores can be represented in the $Im\bar{3}m$ space group. One significant

difference between the resulting structures of SBA-15 and MCM-41 is the unordered micropores which SBA-15 possesses within its walls. Other differences in SBA-15 from MCM-41 include thicker pore walls, larger pores, and higher hydrothermal stability.[6,7]

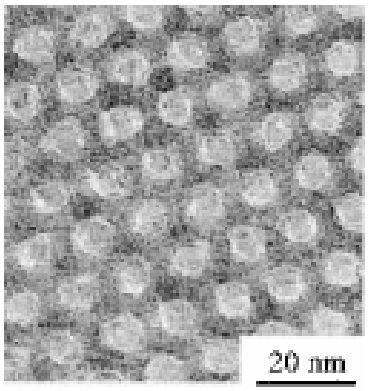

Figure 1.2 TEM image of SBA-15.[7]

1.2.3 KIT-6

KIT-6 is another OMS material developed at the Korea Advanced Institute of Science and Technology in 2003 by Ryoo's group.[8] Its structure is similar to that of MCM-48 in that it can be represented by the *Ia3d* space group. It has pore diameters in the range of 4-12nm. KIT-6 is formed under similar conditions as SBA-15 with the notable difference being the use of butanol as a cosolvent.

1.3 Hybrid Materials

When an inorganic material such as the ones described above are modified with an organic material they are referred to as organic-inorganic hybrid materials or, simply, hybrid materials. Such materials are both physically robust and hold potential to perform

complex separations, highly selective catalysis, and sensing. The property that makes OMS ideal for chemical modification is that the functionalization of silica surfaces is well-developed.[10,11]

1.3.1 Incorporation Methods

In the early 90's, following the development of the M41S materials, a large amount of interest was placed on developing methods for attaching simple organic molecules to the surface of OMS. These studies focused mainly on the attachment of single functional groups, some directly and others indirectly. The ground work for this research was done by Sanchez *et al.* who studied the formation of organic hybridized sol-gels.[12]

In these materials, organic groups are usually introduced *via* an organotrialkoxysiloxane, R-Si(OR')$_3$, where R contains the desired functional group and R' is usually a short alkyl chain such as a methyl or ethyl group. However, mono- or di-alkoxysiloxane may be preferable in some instances. The two approaches for hybridizing OMS are co-condensation and postsynthetic grafting. The co-condensation route involves adding the organotrialkoxysiloxane directly to the synthesis mixture of the OMS and incorpoarated "directly" into the structure. The postsynthetic route involves first synthesizing the OMS then reacting the organotrialkoxysiloxane with the surface silanols, "indirectly" incorporating it into the solid.[11] An example of postsynthetic grafting is shown in Figure 1.3.

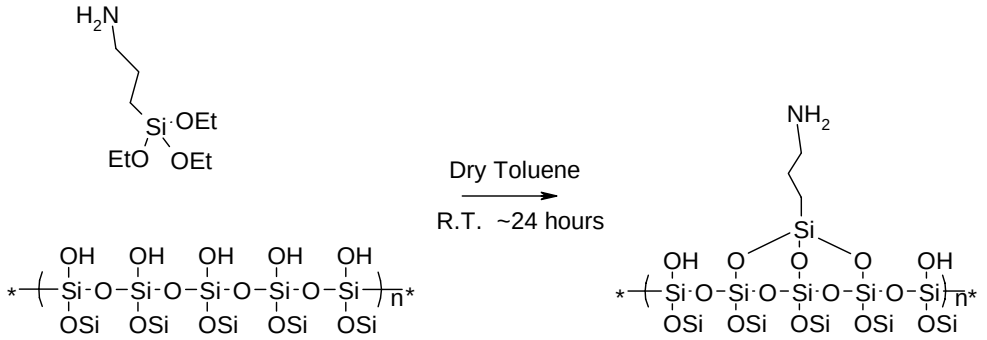

Figure 1.3 Postsynthetic grafting of 4-aminopropyltriethoxysilane (APTES) on silica.

Stein's group compared the advantages and disadvantages of each method for the case of vinyl functionalization of MCM-41.[13] The co-condensation method yielded more uniform functionalization within the pores. The postsynthetically grafted vinyl-MCM-41, on the other hand, was shown to be more hydrothermally stable and the pore characteristics were easier to tune since the organotrialkoxysilane interactions in the synthesis of the OMS were not an issue.

1.3.2 Development

The first hybridized ordered mesoporous silicas were made by Mann's group at the University of Bath.[14] Their work showed that phenyl and *n*-octyl groups could be directly incorporated into MCM-41 by adding phenyltriethoxysilane and *n*-octyltriethoxysilane, respectively, to the synthesis mixture. In 1997, Mann's group published another work showing that amines and thiols groups could be incorporated into MCM-41 using the appropriate organotrialoxysiloxane and hexadecyltrimethylammonium bromide as the structure-directing agent. In the same year, Stein's group attached vinyl to MCM-4 as discussed above.[15] These and several

other functional group incorporations are covered in the review by Moller *et al.* written in 1998.[11] These functionalization methods also apply to SBA-15 and other OMS because the chemistry is the same.[10]

1.3.3 Recent Work

There have been several difficulties involved in forming highly functional well-ordered hybrid materials. These areas have been the focus of most of the recent studies: 1) spatially arranging functional groups; 2) synthesizing hybrids with multiple functional groups; and 3) uniformly incorporating high densities of functional groups.[10]

There have been some successful attempts at dealing with these issues in the past few years. For example, the Jones group at Georgia Tech developed a method for spatially arranging primary amines at relatively high densities on SBA-15 using tritylimine to set the distance between the incorporated groups and then hydrolyzing them to produce primary amines.[16] Mark Davis' group at Cal Tech has also recently developed spatially arranged thiol groups on SBA-15.[17] Lin's group at Iowa State has also shown some progress in directly incorporating multiple functional groups in OMS.[18-20] Progress in developing high densities of uniformly distributed functional groups has been made by incorporating dendrimers in OMS. Work done in this area has been done by Alper and Sayari's labs at the University of Ottawa[21] and my group, the Shantz and Simanek labs, at Texas A&M University.[22] My research focuses on the development of these dendrimer hybridized OMS and their potential applications.

1.3 Dendrimers

Dendrimers are hyperbranched polymers which were first synthesized by D.A. Tomalia and other researchers at the Dow Chemical Corporation in 1979.[23] The word dendrimer comes from the Greek word *dendra*, which means tree, and the scientific term for unit, *mer*. While linear polymers have a fractal dimension of approximately one because they extend on one dimension (unless they are folded), dendrimers have a fractal dimension close to three because they branch out in three dimensions like a tree.

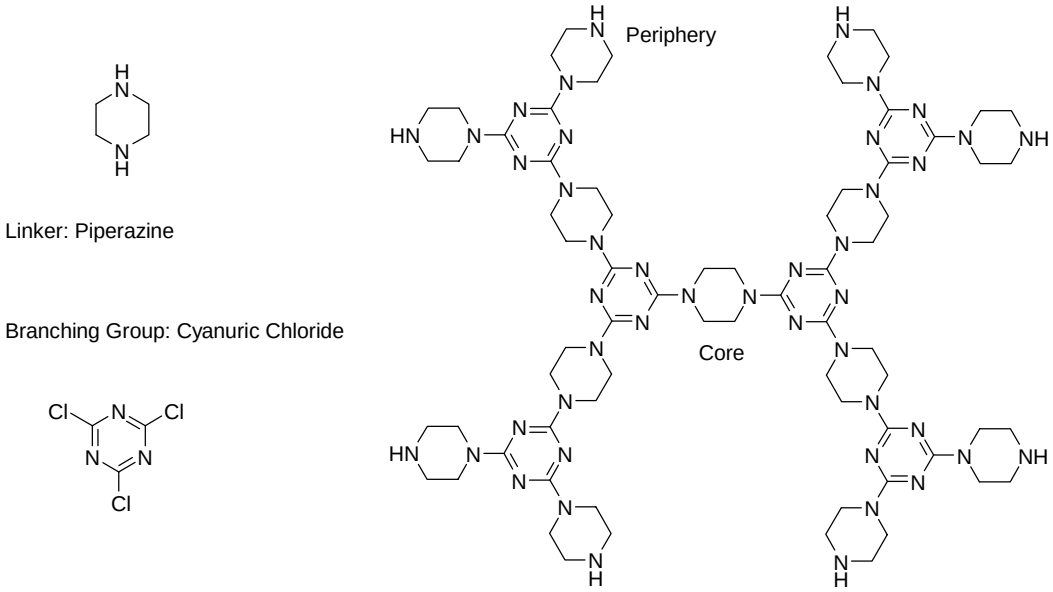

Figure 1.4 A second generation melamine-based dendrimer using a piperazine linker.

1.3.1 Structure

A dendrimer has a "core" at its center as shown in Figure 1.4. Attached to the core are subsequent sets of a "branching group" and "linker" -- or vice versa depending on the chosen core. Each branching group has a linker branching from it which is itself

attached to another branching group in a repeating process.[24] Each branching group/linker set extending out from the core is called a "generation." The terminal ends of a dendrimer are termed "peripheral groups" and are where the promise of dendrimer-hybridized OMS lies. For every generation the number of peripheral groups doubles or triples – depending on the chosen branching group – allowing us to have many functional groups for one covalent bond with the silica surface.

1.3.2 Synthesis Methods

There are two different ways which dendrimers can be synthesized: convergently and divergently. Sometimes, however, it is convenient to use a combination of the two. The convergent method, developed by Frechet *et al.*,[25] begins with the peripheral groups and converges to the core; the divergent method, conversely, starts at the core and diverges out to the periphery. Both of these methods have advantages in certain situations. Of these two methods, it is especially convenient to use the divergent method when synthesizing hybrid materials. Once a proper functional group is attached to the surface of an OMS, one can simply grow the dendrimers off the surface without the necessity of using protecting groups which are usually required in solution dendrimer syntheses.

1.3.3 Melamine-based Dendrimers

An interesting class of dendrimers are those based on melamine or more formally 1,3,5-triazine-2,4,6-triamine (Figure 1.5). These were first developed by Zhang *et al.* in 2000[26] as part of an ongoing series of works pioneered by Eric Simanek's group at Texas

A&M.[22,26-30] The differential reactivity and chemoselective nature of the three reactive sites of 2,4,6-trichloro-1,3,5-triazine (cyanuric chloride, Figure 1.5) make these dendrimers fairly easy to synthesize using various peripheral groups and diamine linkers.[28] Synthesis schemes are simplified by manipulating both temperature and sequence of reactions in order to take advantage of the above properties. This approach dramatically reduces the amount of protecting groups required and, in cases where linkers have two dissimilar amines, can eliminate the need completely.[28]

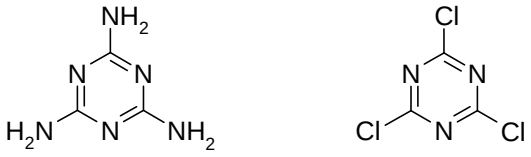

Figure 1.5 Melamine and cyanuric chloride.

1.3.4 Dendrimer Hybrids

The two dendrimer-types which have been used in hybrid OMS materials thus far are melamine-based dendrimers mentioned above[22] and poly(amidoamine) or PAMAM dendrons[21] (Figure 1.6). The syntheses of both dendrimer hybrids begin with amine-functionalization using APTES and end with peripheral primary amines. Both hybrids also use a sequential divergent synthesis approach. The melamine-based dendrimers synthesized by Acosta *et al.* use cyanuric chloride as a branching agent and 4-aminomethylpiperidine as the linker. The PAMAM dendrimers synthesized by Reynhardt *et al.* use ethylenediamine as the branching group and methyl acrylate as the

linker. The Melamine-based dendrimer hybrids developed by Acosta *et al.* will be the focus of this thesis.

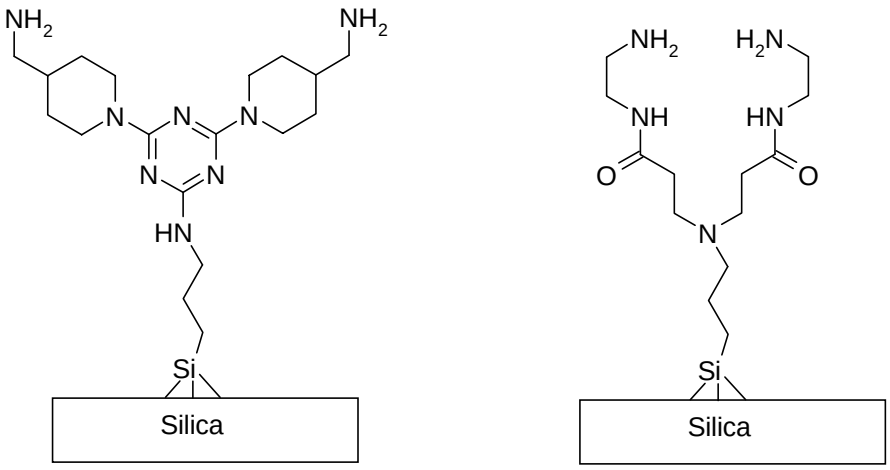

Figure 1.6 First generation dendrimer hybrids: (a) melamine-based (b) PAMAM.

1.4 Enantioselective Catalysis

The second part of this thesis is focused on is how we can take our knowledge of hybrid materials and apply it to catalysis.

1.4.1 Historical Development

For almost a century, since the Germans used the *Haber-Bosch* process to synthesize ammonia from nitrogen and hydrogen in WWI and *Fischer-Tropsch* synthesis to make hydrocarbons from coal in WWII using iron catalysts, chemists and engineers have been fascinated by the use of catalysts and have sought to develop increasingly better ones for a wide variety of chemistries. Today, almost every industrial scale reaction uses catalysts, either bound to a support or present in some other form.

Conventionally, small metal particles (several nanometers in diameter) were dispersed into an amorphous solid to increase the exposed surface area of the catalytic metal and reduce costs. However, in more complex chemistry these metal catalysts have low selectivity for the desired product and are still quite expensive.

Efforts to employ metal ions in zeolitic frameworks were prevalent in the early 90's.[31-36] Though, these materials show great catalytic activity, their use is limited by their small pore size as mentioned above. Upon the introduction of ordered mesoporous silicas, there was – and still remains – interest in attaching metals and organometallic complexes to these surfaces to increase the selectivity and take advantage of the larger pore size.[10,37-39]

Though in many cases metals and metal complexes are useful catalysts, metal leaching can be an issue, causing contamination in the product stream, an environmental hazard, and reducing the life of the catalyst. Metal leaching is particularly problematic in the pharmaceutical and fine chemicals industries, where trace metal contamination is unacceptable. One of the largest problems that manufacturers must deal with in addition to metal leaching is producing enantiomerically pure products. Due to this requirement, drug companies spend a great deal on separations.

1.4.2 Enantiomers

An enantiomer is one of a set of two chiral isomers which are mirror images of each other as shown in Figure 1.7. Something that is termed chiral has no planes of symmetry. A simple example of enantiomers are the human hands. If you look at one hand, there is no way that it can be split so that it will produce two or more equal

portions; your hand is chiral. When you look at your other hand and compare the two, they are exact mirror images which cannot be superimposed; your hands are enantiomeric partners. A chiral compound's orientation can be determined using the Cahn-Ingold-Prelog priority rules. The effects of the two enantiomers on the human body are different, even though they are chemically the same. In many cases, the "incorrect" enantiomer can have detrimental effects on the body and its ability to utilize the "correct" enantiomer.[40]

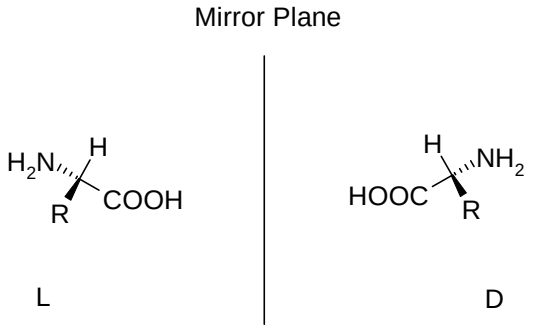

Figure 1.7 Structural comparison of an enantiomeric pair of amino acids. R is the side chain.

1.4.3 Recent Trends

A trend in recent years has been to use enzymes as catalysts because they are highly selective and can produce enantiomerically pure products. Enzymes, however, are expensive and extremely sensitive to temperature, pH and sheer stress. These complications have led a number of researchers to search for viable enzyme mimics.[41-43]

1.4.4 L-Proline

One potential enzyme mimic is the amino acid L-proline. The catalytic properties of L-proline have been known since it was studied in 1971 by Eder, Sauer and Wiechert[44] and in 1974 by Hajos *et al.*[45] as a catalyst for what is now called the Hajos-Eder-Sauer-Wiechert reaction (Figure 1.8).

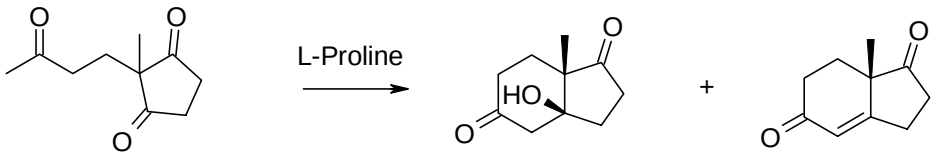

Figure 1.8 The Hajos-Eder-Sauer-Wiechert reaction.

It went virtually forgotten until recently when Benjamin List *et al.* studied it as a potential class I aldolase mimic.[46] They showed that it could be used as an enantioselective catalyst in aldol reactions including that shown in Figure 1.9. List *et al.* showed again in the same year the potential for L-proline in Mannich reactions [47] and has since then produced many others.[48-51] Barbas *et al.* have also studied L-proline in these reactions as well as Michael and Diels-Alder reactions.[48,52-55] List *et al.* have proposed an enamine catalysis mechanism while some others have believed there is a cooperative effect between multiple L-proline molecules.[46,51,56-58] However, there has yet to be a definitive mechanism developed.

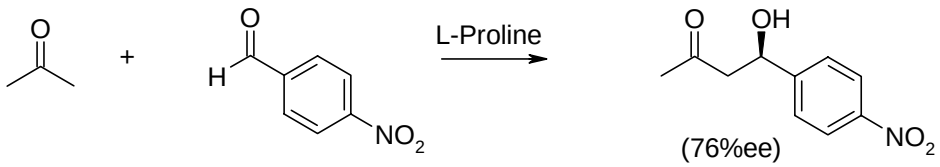

Figure 1.9 Aldol reaction of *p*-nitrobenzaldehyde and acetone.[46] Note that with L-proline as the catalyst, one enantiomer is favored over the other.

1.5.4 Proline Hybrids

There has only been one report on L-proline/silica hybrids performed by Dhar *et al.* at the Indian Institute of science.[59] In that study, L-proline was attached to MCM-41 using isocyanatopropyl triethoxysilane. For the reaction shown in Figure 1.9, a yield of 36% and 59% *ee* were obtained. In addition to this study, several others were performed by Benaglia *et al.* grafting L-proline to polyethylene glycol.[60,61]

1.6 Objectives and Hypotheses

The objective of this research was to take the work done by Acosta *et al.* on melamine-based dendrimer hybrids and further develop this system so that the pore size, pore volume, surface area, and chemical functionality can be tuned independently. Furthermore, the application of this system in the area of enantioselective catalysis will be studied in order to develop a functional heterogeneous catalyst for aldol and Mannich reactions using L-proline.

From the above background material, several hypotheses were been made and have be studied in order to meet the set objectives: 1) SBA-15 is a model hybrid support due to its large pore size and ordered hexagonal pore structure; 2) melamine-based

dendrimers are a potential route to increase the density of functional groups in hybrid materials; 3) the pore size and volume can be tuned by changing the choice of linker in melamine-based dendrimer hybrids; 4) these hybrids have potential for separations such as metal sequestering; 5) they can also serve as an ideal heterogeneous support for an enantioselective organocatalyst using L-proline.

CHAPTER II

METHODS

2.1 Introduction

Due to the complexity of dendrimer/SBA-15 hybrid materials, many analytical methods are required to understand them such as X-ray diffraction (XRD), porosimetry, thermal gravimetric analysis (TGA) and infrared spectroscopy (IR). The most important of these methods are X-ray diffraction and porosimetry. X-ray diffraction provides information about the structure and level of organization of the inorganic material; Porosimetry provides information concerning the pore size distributions, pore volume and surface area of the combined material, before and after organic functionalization.

In addition to these techniques, other tools are required when performing organic syntheses and performing enantioselective catalysis experiments such as nuclear magnetic resonance (NMR), mass spectroscopy (MS) and chiral gas chromatography. Chiral gas chromatography is an important tool that can be used to determine the degree of enantioselectivity of a given catalyst.

2.2 Powder X-Ray Diffraction

X-ray diffraction is important for characterizing the nanostructure in OMS. These materials are powders (~1μm) so single-crystal diffraction methods are not applicable. In powder X-ray diffraction (PXRD), in contrast to single-crystal methods, the particles are randomly oriented such that all the crystal planes face the X-ray beam. Though OMS is

not crystalline, the mesopores possess long range order which give rise to Bragg diffraction peaks.

The X-rays used are typically from bombarding either copper (Cu) or molybdenum (Mo) with high energy electrons, though in principle almost any metal could be used. The emitted X-rays are then filtered or passed through a monochromater to produce Kα radiation from the respective metal. CuKα possesses a wavelength of 1.541 Å and MoKα possesses a wavelength of 0.709 Å. Once the X-rays impinge on the sample, they diffract off of each of the exposed planes and a detector rotates around the sample recording the intensities of diffraction at each angle. There are other instrument geometries, however, this arrangement is the one used here. The diffraction peak intensities are plotted as a function of 2θ, where θ is the angle of diffraction. The angles at which the peaks are observed can be used to determine the interplanar spacing of atoms (periodicity) or *d*-spacing for each crystal plane using Bragg's Law (See Figure 2.1). For OMS, these values can be used to estimate the unit cell dimensions of the pore arrangements. Bragg's Law can be expressed as the following:

$$n\lambda = 2d\sin(\theta) \qquad (2.1)$$

where

λ = the wavelength of the monochromatic X-ray beam, [L]

n = some integer 1, 2, 3…

θ = the angle of incidence, [radians]

d = the interplaner spacing of atoms, [L]

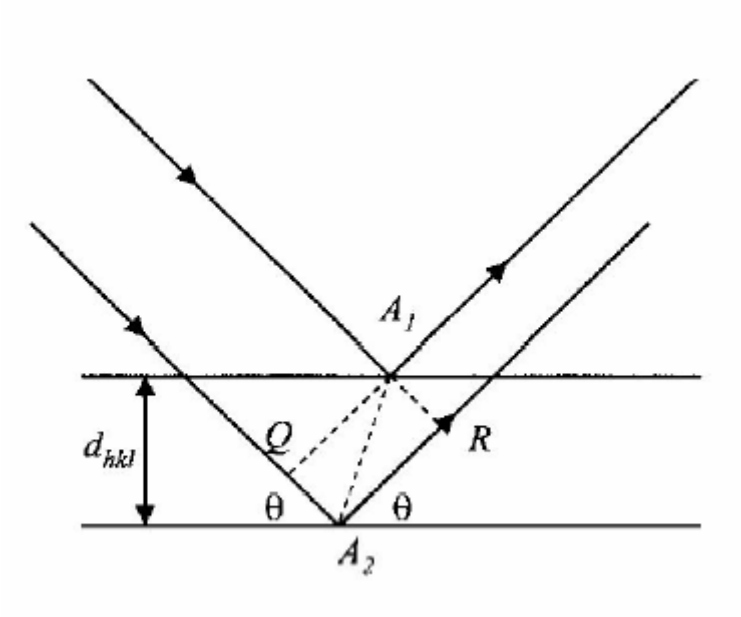

Figure 2.1 A visual representation of Bragg's Law.[62]

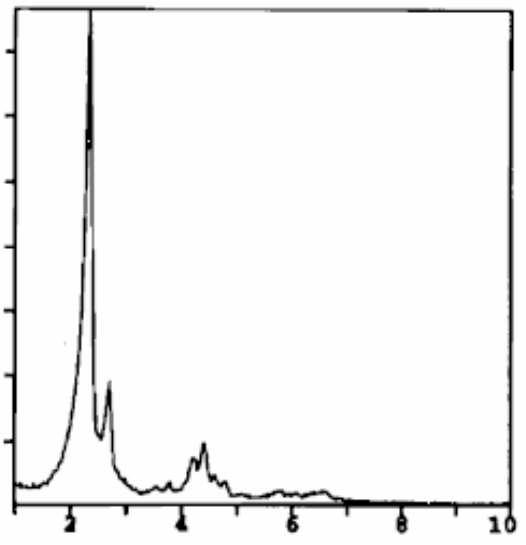

Figure 2.2 The XRD pattern of MCM-48.[3]

By comparing the positions of the peaks versus 2θ and knowing the pore topology/symmetry, one can assign Miller indices – which are related to a plane of reflection – to a peak and derive the unit cell parameters. The unit cell parameters for OMS are related to the distance between the repeating arrangement of the pores (i.e. hexagonal, cubic, etc.). For well-studied OMS, such as MCM-41 (Figure 2.2) or SBA-15, a comparison between peak values gathered during experiment and known relationships between peaks obtained in the literature is all that one must do to identify the structure.

2.3 Adsorption (Porosimetry)

Nitrogen physisorption is one of the most common methods used to determine the pore size distribution, surface area, and pore volume in porous materials and will be the method used here to characterize OMS and OMS hybrids. Physisorption differs from chemisoption in that it is adsorption due to van der Waals forces rather than chemical bonding, it is reversible, and can form multiple layers whereas chemisorption is inherently restricted to a monolayer.[1] These differences make physisorption a good method for probing the internal structure of porous materials. Such measurements are usually done at the boiling point of the analysis gas (77 K for nitrogen).

There are six classifications of physisorption isotherms as shown in Figure 2.3.[1] A Type I isotherm is indicative of a microporous structure. Type II is the isotherm of a non-porous solid. Type IV is a mesoporous solid and is the isotherm type with which the analyses in this thesis shall deal. Types III, V and VI are uncommon and will not be discussed.

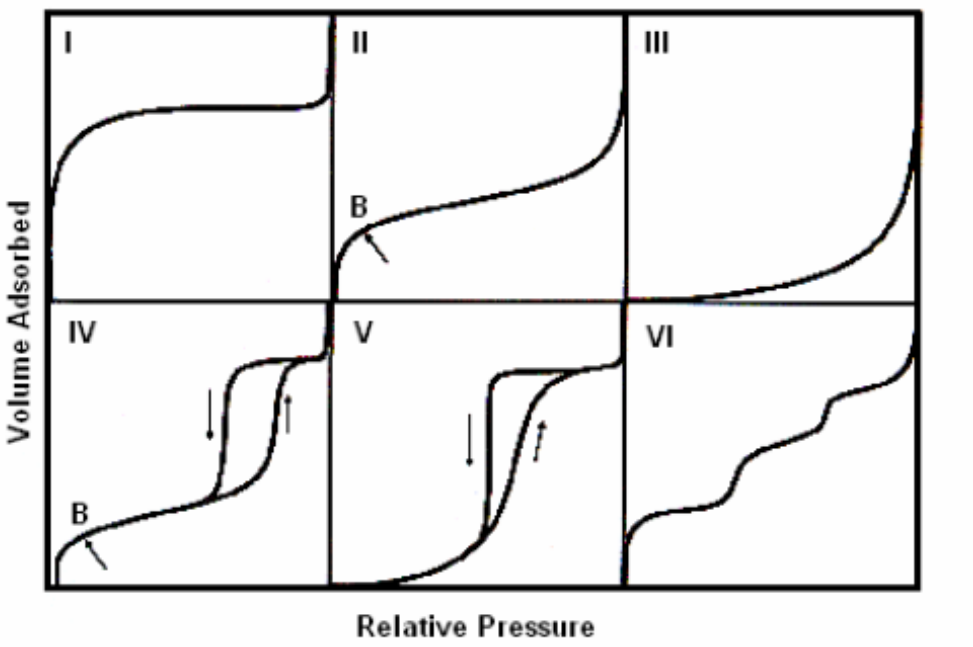

Figure 2.3 The six IUPAC adsorption isotherm classifications.[1]

2.3.1 α_s analysis

α_s analysis is a method which can be used to extract information about the pore volume and surface area from an adsorption isotherm. The α_s method is a variant of the t-plot method with a few important differences.[1] First, in contrast with the t-plot method, the absorbate monolayer thickness does not need to be estimated. Second, the analyzed sample is compared with a non-porous reference material. The differences between the two materials result from the effects of micro- and mesopore filling. The key assumption in this method is that the surface chemistry of the reference material is the same as the analyzed sample. Another popular model is the BET (Brunauer, Emmett, and Teller) method. This method also has several disadvantages compared to α_s analysis. The BET method usually requires at least an estimate of the volume adsorbed at monolayer coverage whereas the α_s method makes no other assumption than the one stated above.

In the α_s approach, the isotherm is non-dimensionalized the isotherm (volume adsorbed versus relative pressure, p/p_0) by dividing the volume adsorbed (v_{exp}) at each relative pressure by the volume adsorbed at $p/p_0 = 0.4$ and redefining this value as α_s.

$$\alpha_s = \frac{v_{\exp}}{v_{\exp, p/p_0 = 0.4}} \tag{2.2}$$

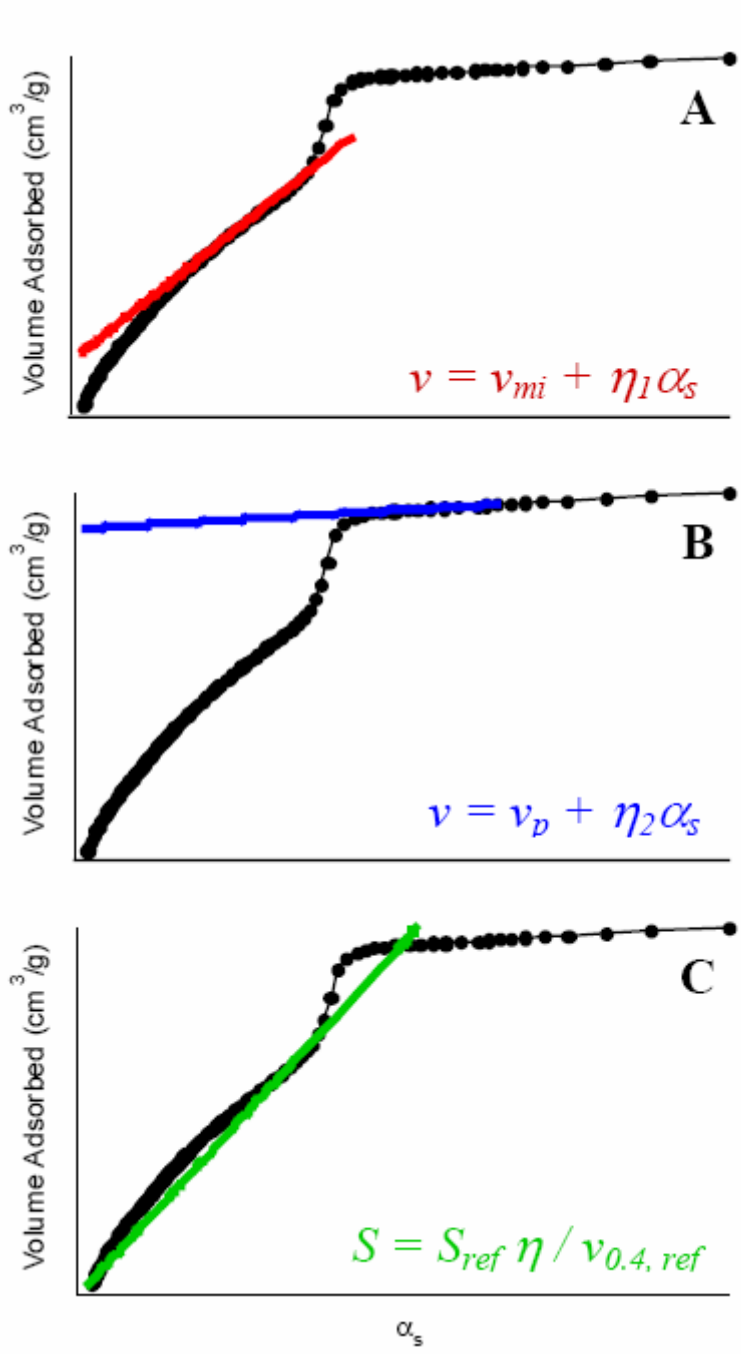

Figure 2.4 α_s analysis of a type I isotherm.[63]

An equation for this isotherm, $\alpha_s(p/p_0)$ can be fitted to the data by employing common curve fitting techniques. Using this equation, one can construct a plot of the volume of probe gas adsorbed versus α_s, (Figure 2.4). A sample which is nonporous would exhibit a straight line. Conversely, areas of nonlinearity indicate porosity. It is from these sections that data can be obtained concerning pore volume and surface area.

The pore volume information is determined by drawing tangent lines to each nonlinear section of the isotherm and extrapolating them back to the y-axis.[1] The intercept of the tangent line to the first section is the micropore volume. For an OMS such as SBA-15 which has micropore and mesopores, the next section's tangent line will have the total pore volume as its intercept. The mesopore volume can be determined by subtracting these two values. The surface area can be determined by knowing the slope from the origin to the point at a relative pressure of 0.4 and substituting it into the equation:

$$S = \frac{S_{ref}\eta}{v_{p/p_0=0.4}} \tag{2.3}$$

where

S = the surface area

v = the volume adsorbed

η = the slope

2.3.2 BJH Analysis

The Barret-Joyner-Halenda (BJH) analysis[64], which is derived from the Kelvin equation, is commonly used to determine the pore size distribution in mesoporous solids. Assuming cylindrical pores, which is the case for most OMS, and using parameters developed in 1997 by Jaroniec *et al.*[65] the pore size distribution can be estimated with the expression:

$$r(p/p_0) = \frac{\gamma V_L}{RT \ln(p/p_0)} + t(p/p_0) + 0.3 \qquad (2.4)$$

$$t(p/p_0) = 0.1\left[\frac{60.65}{0.03071 - \log(p/p_0)}\right]^{0.3968} \qquad (2.5)$$

where

V_L = the molar volume of liquid adsorbate

γ = the surface tension of the liquid adsorbate

t = the liquid film thickness

2.4 Chiral Gas Chromatography

2.4.1 Theory

Chiral Gas Chromatography (CGC) is used to separate molecules by exploiting stereochemistry -- in addition to dispersion, polar and ionic interaction differences --with

a chiral stationary phase.[66] Other than the use of a chiral stationary phase, the theory and set up of a CGC is the same as normal gas chromatography (GC).[66] Compounds dissolved in a solution are injected into a column at an elevated temperature, evaporated, and carried through the column by a carrier gas, usually helium, and separated from each other due to different interactions with the column resin.

The basis for the separation of two compounds A and B in the column is the ratio of their respective distribution coefficients. This value is called the separation ratio and is shown in equation 2.6.

$$\alpha_{AB} = \frac{K_A}{K_B} \tag{2.6}$$

where

α_{AB} = the separation ratio between components A and B

K_i = the distribution coefficient of component *i* between the mobile and stationary phases

This distribution coefficient is a function of the difference in the Gibbs free energy between both states. The Gibb's free energy is itself a function of enthalpy and entropy.

$$RT \ln K_i = -\Delta G_{i0} \tag{2.7}$$

and

$$\ln K_i = \frac{-\Delta H_{i0}}{RT} + \frac{\Delta S_{i0}}{R} \tag{2.8}$$

where

R = the universal gas constant

T = the absolute temperature

ΔG_0 = the standard Gibb's free energy

ΔH_0 = the standard enthalpy change

ΔS_0 = the standard entropy change

So, the distribution coefficient is a function of both entropy and enthalpy.

In general, the entropic component can be neglected because the enthalpic component is large in comparison. Contributions to the enthalpic component include the interactions listed above: dispersion, polar and ionic forces. These separations are said to be enthalpically-driven. However, for enantiomers in a chiral column where the separation is predominantly based on size exclusion, the entropic component becomes the major contributor toward the separation and enthalpic effects become negligible; the enantiomer which shares the same orientation as the stationary phase will have more access to it. This type of separation is said to be entropically-driven. A more realistic situation for separating enantiomers is one where both enthalpy and entropy components are important. The enantiomer which shares the stationary phase orientation will have more access to it (entropy) and as a result have stronger interactions with the surface functional groups (enthalpy).

2.4.2 Stationary Phases

Though other stationary phases have been used, including those based on amino acid and polysiloxane derivatives, the most common chiral stationary phases used today are α-, β- and γ-cyclodextrin and its derivatives.[66] Cyclodextrins are cyclic polymers of D-glucose units joined by α-(1-4)glycosidic linkages. α-, β-, and γ-cyclodextrin have six, seven and eight glucose units, respectively (Figure 2.4). Their overall shape is similar to

a cross-section of a hollow cone where the opening at the top is wider than at the bottom. The three cyclodextrin structures vary in the diameter of their mouth openings. α-, β- and γ-cyclodextrin have openings of 5.7 Å, 7.8 Å and 9.5 Å, respectively[67] (Figures 2.5 and 2.6). The glucose units are configured in such a way that both secondary hydroxyl groups are exposed at the wider opening and the primary hydroxyl group is exposed at the smaller opening.

The reason that these macromolecules are so widely used is due to the high density of chiral centers, while at the same time their structure allows them to entrap small molecules in their central cavity. Each D-glucose unit has 5 chiral centers, so γ-cyclodextrin has a total of 40 chiral centers with which components in the mobile can interact. The hydroxyl groups on both ends can also be modified to engineer the resin for a specific separation. The cyclodextrin used in the chiral column for this research is trifluoroacetyl derivatized γ-cyclodextrin.

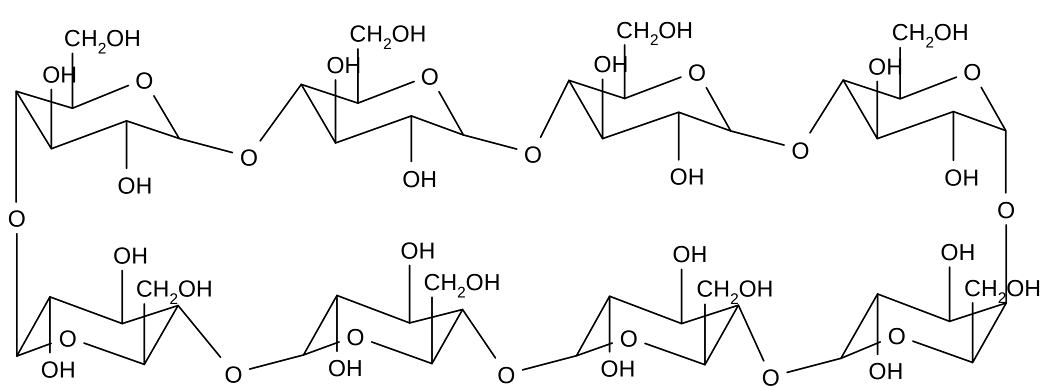

Figure 2.5 Structure of γ-cyclodextrin.

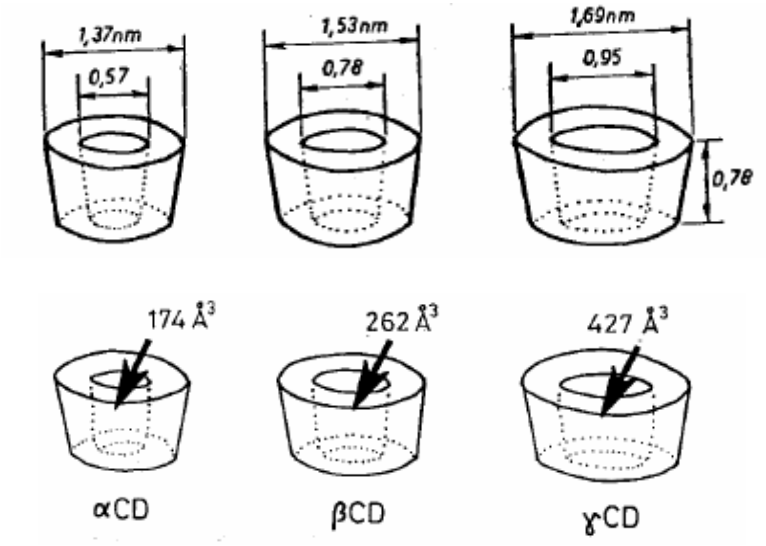

Figure 2.6 Shapes and sizes of α, β, and γ cyclodextrin (CD).[67]

2.2.3 Enantiomeric Excess Determination

When evaluating a new asymmetric catalyst, one of the most important characteristics is its enantioselectivity. CGC can be used to estimate the enantiomeric excess of one enantiomer (Equation 2.9) in the reaction product by comparing the areas under the two peaks in the resulting chromatograph. The enantiomeric excess is defined and can be estimated by the following:

$$ee = 100\left(\frac{N_R - N_S}{N_R + N_S}\right) \tag{2.9}$$

where

ee = the enantiomeric excess of enantiomer R [%]

N_i = the number of moles of component i

Equation 2.9 is related to experimental measurements using CGC by comparing the areas under the two peaks in the resulting chromatograph as shown in Equation 3.0.

$$ee \approx 100\left(\frac{A_R - A_S}{A_R + A_S}\right) \tag{3.0}$$

where

A_i = the area under the chromatograph curve of component on i

CHAPTER III

MELAMINE DENDRIMER/SBA-15 HYBRIDS

3.1 Introduction

As mentioned above, to date there have been only two reports of dendrimers covalently attached to OMS: melamine-based dendrimers synthesized on SBA-15 by Acosta *et al.* [22] and PAMAM dendrimers synthesized on MCM-41 by Reynhardt *et al*.[21] This investigation builds off of the work of Acosta *et al.*, expanding the scope of these systems to other linkers in the dendrimers, as well as demonstrating that these materials can be used in such applications as metal sequestration. A thorough characterization study is presented using a variety of methods to determine the hybrid microstructure.

3.2 Experimental Method

3.2.1 Materials

Tetraethoxysilane (TEOS, ≥ 99%) was purchased from Fluka. Pluronic P123 ($EO_{20}PO_{70}EO_{20}$, MW=5800) was obtained from BASF. Ethanol and toluene (ACS reagent grade) were purchased from EM Science. 3-aminopropyltriethoxysilane (APTES, 99%), Piperazine (P, 99%), 4,4'-Trimethylenedipiperidine (TMDP, 97%), and N,N-diisopropylethylamine (DIPEA, 99%) were purchased from Aldrich. 4-(aminomethyl)piperidine (AMP, ≥ 98%) was purchased from TCI America. Cyanuric Chloride (CC, 99%) was purchased from ACROS. Tetrahydrofuran (THF), methanol, and dichloromethane (DCM) (all ACS reagent grade) were purchased from EMD. Copper(II)sulfate pentahydrate (Cupric Sulfate, ≥ 99%) was purchased from J.T. Baker.

Ethylenediamine-tetraacetic acid disodium salt (EDTA, ≥ 99%) was purchased from EM Science. Murexide (Ammonium Purpurate) was purchased from ACROS. All chemicals were used as received.

3.2.2 Synthesis of Amine-functionalized SBA-15

SBA-15 was synthesized using a method comparable to that reported previously.[6] 4.0 g of Pluronic P123 were dissolved in 60 mL of 4M HCl and 85 mL of deionized water by stirring for 5 hours at room temperature. Then 8.5 g of TEOS were added to that solution and stirred for 24 hours at 35 °C. The mixture was aged at 80 °C for 24 h under static conditions. The solid product was filtered, washed with copious quantities of deionized water and air-dried overnight.

The solid product was calcined to remove the polymer used in the synthesis. The calcination procedure was as follows: the sample was heated from room temperature to 100 °C at a rate of 1 °C/min; held at 100 °C for 1 hour; increased from 100 °C to 500 °C at a rate of 1 °C/min; and then held at 500 °C for 5 hours. The amine-functionalized SBA-15 was prepared using post-synthetic grafting. An aliquot of APTES 16 μL (0.1 mmol), 80 μL (0.5 mmol), 160 μL (1.0 mmol) or 320 μL (2.0 mmol), depending on the desired amine loading, was added to 1 g of calcined SBA-15 in 100 ml of anhydrous toluene under nitrogen. This mixture was stirred overnight in a closed container at room temperature. The product was collected by filtration, washed with 1 L deionized water and air-dried.

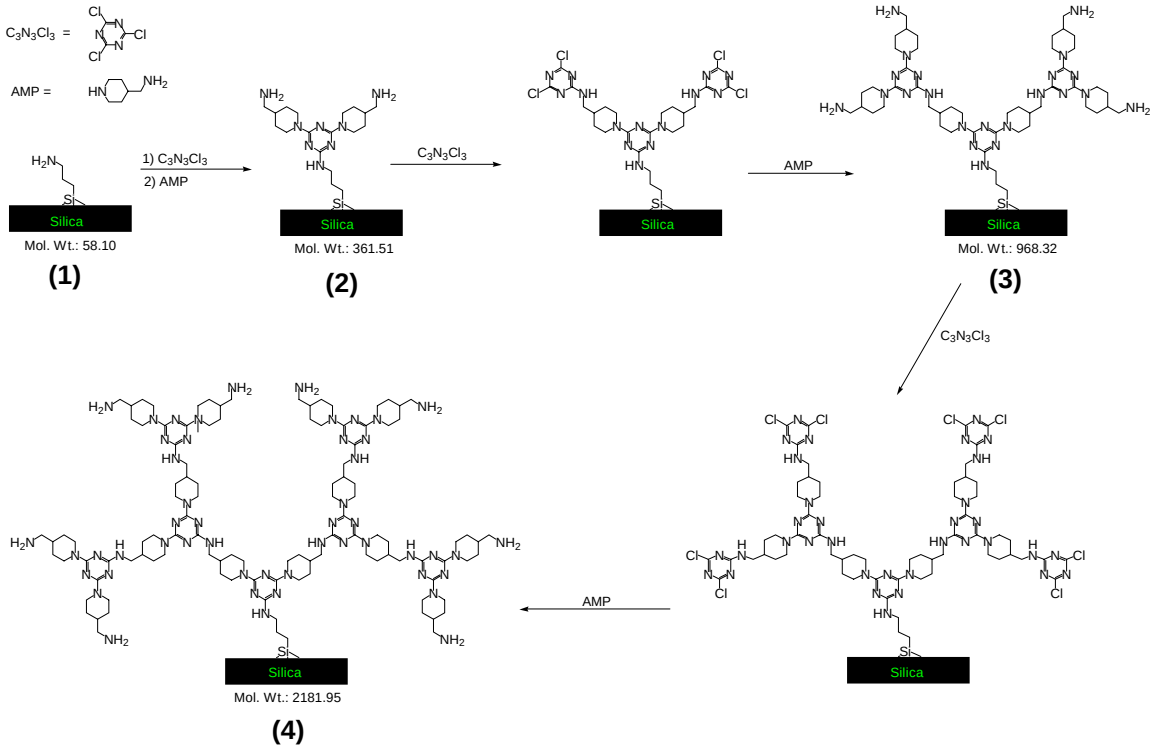

Figure 3.1 Iterative synthesis of melamine-based dendrimer hybrids. The syntheses of the first three generations are shown: (**1**) Amine-functionalized SBA-15, (**2**) G1-AMP dendrimer, (**3**) G2-AMP dendrimer, (**4**) G3-AMP dendrimer.

3.2.3 Synthesis of Dendrimer/SBA-15 hybrids

The synthesis of the hybrids is illustrated in Figure 3.1. A 0.3 M cyanuric chloride (CC) solution was prepared by adding 1.25g CC and 2.5 mL diisopropylethylamine (DIPEA) (8mmol) to 25 mL of tetrahydrofuran (THF). A 0.4 M 4-(aminomethyl)piperidine (AMP) solution was prepared by adding 1.25 g AMP to 25 mL of THF. 0.4 M solutions were also prepared for piperazine (P) and 4,4'-trimethylenedipiperidine (TMDP) in a similar manner. One gram of amine-functionalized SBA-15 was placed in a 30 mL vial and 25 mL of the prepared CC solution are added. The vial was shaken for approximately 24 hours at room temperature. The solution was filtered to remove the silica from the solution and the silica was rinsed with 50 mL portions of methanol, dichloromethane, and THF sequentially. The silica was transferred back into a clean vial, 25 mL of the linker molecule solution were added, and the vial is again shaken for 24 hours. The material was filtered and rinsed as described above. The same procedure was followed to increase the dendrimer generation. So that every dendrimer has the same functionality on the outer periphery (primary amine), the final linker molecule added to each sample was AMP. Figure 3.2 illustrates the second-generation dendrimer for each linker molecule.

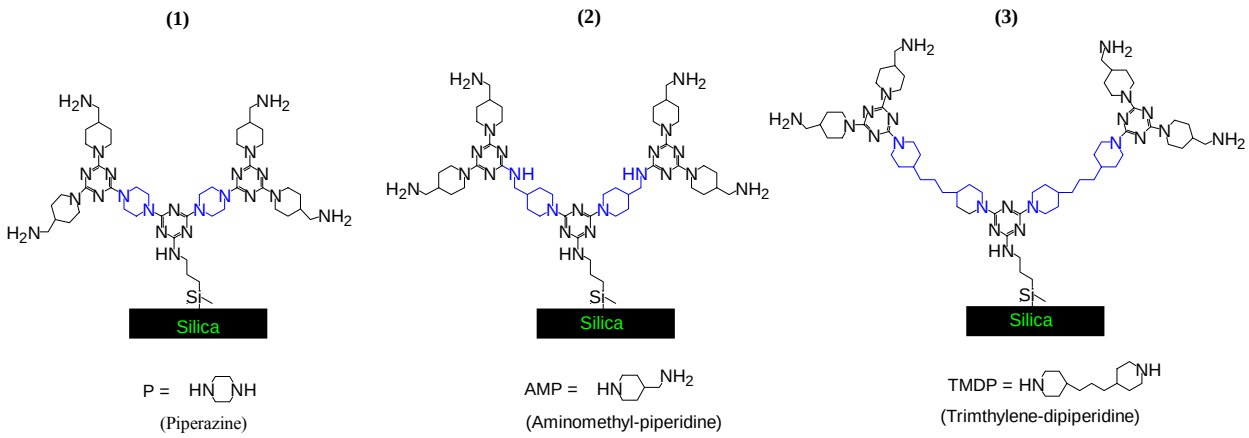

Figure 3.2 Dendrimer/SBA-15 hybrids using different linkers. (**1**), (**2**), and (**3**) use the linkers P, AMP, and TMDP, respectively. Second generation dendrimers are shown in all cases.

3.2.4 Analytical

Powder X-ray diffraction (PXRD) measurements were performed using a Bruker-AXS D8 powder diffractometer with Cu Kα radiation over a range of 0.8 to 5° 2θ. Peak intensities and 2θ values were determined using the Bruker program EVA. Transmission electron microscopy (TEM) was performed on a JEOL 2010 microscope with a lanthanum hexaboride filament and an excitation voltage of 200 kV. Infrared spectroscopy was performed on the G3 hybrids, Amine-SBA-15 and SBA-15 using a Nexus 670 FT-IR Spectrometer from Thermo Nicolet. Thermal gravimetric analyses (TGA) were performed using a TG 209C Iris Instrument from Netsch over a temperature range of 25 to 515 °C using oxygen as a carrier gas and temperature ramping rate of 5 °C min^{-1}. Nitrogen adsorption experiments were performed on a Micromeritics ASAP 2010 micropore system using approximately 0.1 g of sample. The samples were degassed under vacuum at room temperature for 2 h, then at 40 °C for 4 h, then at 60 °C for 4 h before analysis. The micropore and mesopore volumes were determined using the α_s-method.[1,68] The mesoporous size distributions were calculated from the adsorption branch of the isotherm using the Barret-Joyner-Halenda (BJH) method[64] with a modified equation[65] for the statistical film thickness.

3.2.5 Copper(II) Sequestration

30 mg of the following samples were placed in vials: bare SBA-15, 0.5 mmol/g amine-SBA-15, and G1, G2, and G3 AMP-based hybrids (0.5 mmol/g amine loading). To these vials 6.6 mL of 14.4mM cupric sulfate in purified water (360.0 mg of cupric sulfate pentahydrate per 100 mL water) were added. The mixtures were then shaken for

14 hours. The resulting solutions were filtered and 2 mL of each were titrated with 5.4mM Na_2EDTA using murexide as the indicator (50.2 mg per 100mL purified water). Each solution was titrated twice including the stock cupric sulfate solution.

3.3 Results and Discussion

3.3.1 PXRD/TEM

Powder X-ray diffraction was used to characterize the structure of the dendrimer-SBA15 hybrid materials. XRD patterns for each generation are shown in Figure 3.3. The parent SBA-15, amine-SBA-15 and G1-hybrid materials show three well-defined peaks at 2θ values between 0.8 to 5° that can be indexed as the (100), (110), and (200) Bragg peaks, typical of hexagonal (*p6mm*) SBA-15.[6] The (100) peak is clearly observed as the dendrimer generation increases, however the intensity of (110) and (200) peaks decrease for the G2 and G3 hybrids. Subsequently TEM was used to verify the SBA-15 retained its structural ordering. The images in Figure 3.4 show that that mesostructure is hexagonally ordered as expected.

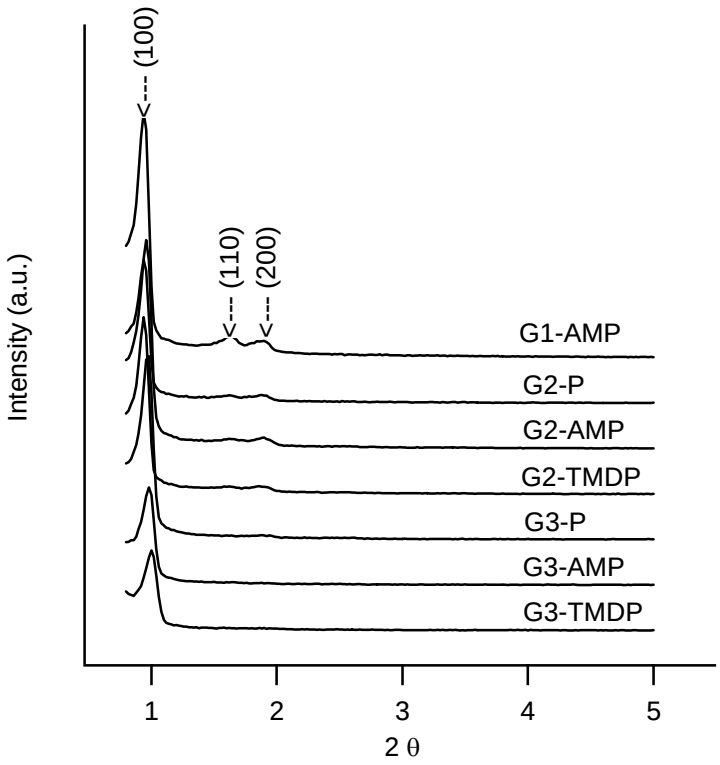

Figure 3.3 PXRD pattern for dendrimer/SBA-15 hybrids.

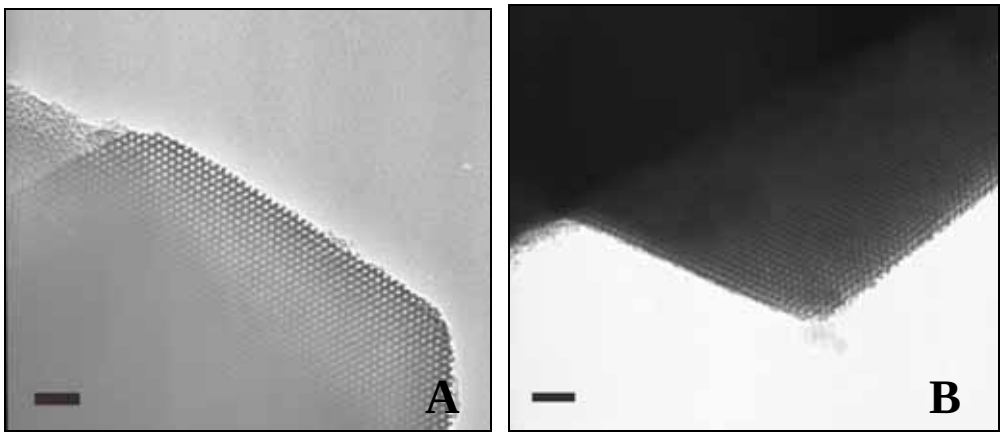

Figure 3.4 TEM of (A) G3-AMP-SBA15 and (B) G3-TMDP-SBA15. The scale bars in the figures correspond to 50 nm.

3.3.2 Infrared Spectroscopy

Infrared spectroscopy was used to verify the presence of the dendrimers. Figure 3.5 shows the spectra for SBA-15, amine-functionalized SBA-15 and the G3 hybrids of each linker molecule. The spectra show the G3 hybrids are chemically different from SBA-15, the amine-SBA-15, and each other. The spectra exhibit the characteristic peaks for the primary, secondary and tertiary carbon C-H bond stretches between 2800 and 3000 cm^{-1}. These peaks are not observed in the parent SBA-15 sample, and are very weak for the amine-SBA-15 hybrid. The intensity differences between the samples are due to the different linker molecules in the dendrimers. The dendrimer-hybrids also show aromatic peaks between 1400 and 1600 cm^{-1}. The results are qualitative evidence for hybrid formation. The dendrimer content is quantified using thermal gravimetric analysis (TGA).

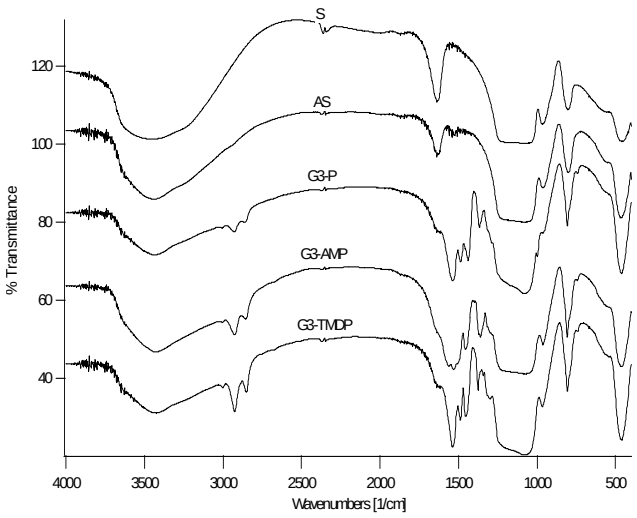

Figure 3.5 IR spectra of SBA-15, Amine-SBA-15 and G3 hybrids. SBA-15 (S), 0.5mmol Amine-SBA-15 (AS), G3-P, G3-AMP, and G3-TMDP are shown.

3.3.3 TGA

TGA was used to determine the organic content of each dendrimer-SBA15 hybrid and to estimate the yield of adding each generation. The TGA results are summarized in Table 3.1. The weight percent of organic increases by approximately 10% for one generation increase of AMP: 11*wt*% for G1, 20*wt*% for G2, and 31*wt*% for G3 (See Figure 3.6). The step yieldss for the AMP-based hybrid are 31%, 75%, and 83% for the syntheses of the G1 dendrimer from amine-functionalized SBA-15, the G2 dendrimer from the G1 dendrimer, and the G3 dendrimer from the G2 dendrimer, respectively. The step yields for P and TMDP–based hybrids also increase with generation size: 71% and 91% for the second and third generation of P and 70% and 115% for the second and third generation of TMDP. However, theses two sets are not completely comparable with the AMP-based hybrids because the final linker molecule on both sets is AMP rather than P or TMDP, as stated above. The 115% yield for the last step in the G3-TMDP hybrid is probably a result of AMP being more reactive than TMDP and reacting with many of the triazines which remained unreacted.

Based on the TGA results some trends are also observed as the linker group is varied. The increase in organic content per generation is approximately 8*wt*% for P, 10*wt*% for AMP, and 9*wt*% for TMDP. The result for piperazine is expected because it is a smaller molecule than AMP and contributes less to the overall organic content. TMDP, however, does not behave as expected, as the organic content for a given dendrimer generation should be larger for this linker than with AMP or P. This is likely due to the fact that TMDP does not react as quantitatively as AMP with either the preceding dichlorotriazine or the following cyanuric chloride.

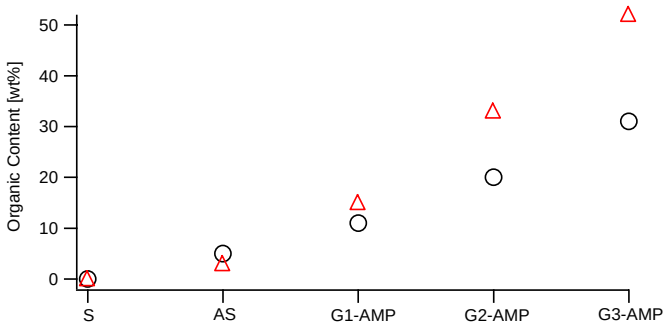

Figure 3.6 TGA results for hybrids using AMP. The organic contents are shown for SBA-15 (S), 0.5mmol/g Amine-SBA-15 (AS), G1-AMP hybrid, G2-AMP hybrid, and G3-AMP hybrid: (Δ) values for 100% yield at each step; (O) actual values**.**

Table 3.1 TGA data: (A) dendrimers size effects; (B) amine loading effects

(A)

Sample ID	Organic* [wt%]	Organic [mmol/g SBA-15]	Step Yield†
0.5 mmol Amine	5%	0.97	-----
G2 P	19%	0.24	71%
G3 P	27%	0.21	91%
G1 AMP	11%	0.34	31%
G2 AMP	20%	0.25	75%
G3 AMP	31%	0.21	83%
G2 TMDP	20%	0.24	70%
G3 TMDP	29%	0.27	115%

(B)

Sample ID	Organic [wt%]	Organic [mmol/g SBA-15]
0.1 mmol Amine	3%	0.54
G3 AMP (0.1 mmol)	17%	0.10
1.0 mmol Amine	8%	1.41
G3 AMP (1.0 mmol)	38%	0.28
2.0 mmol Amine	8%	1.48
G3 AMP (2.0 mmol)	39%	0.29

* These numbers do not reflect that the bare SBA-15 has a weight loss between 2.5-4.5 wt% in the same temperature range. The numbers have not been "subtracted" or "corrected" for this.

† The step yield is calculated based on the initial amount of the previous dendrimer (i.e. in going from G1 → G2, it is based on the G1 content as determined by TGA)

TGA results for the varied amine-loadings (Table 3.1B) show that the amine loading can be increased or decreased without greatly influencing the overall yield of the G3 dendrimer growth: 24% for 0.1 mmol/g and 20% for 2.0 mmol/g. However, it is worth noting that the amount of amine deposited in the 1.0 mmol/g sample is the same as that for the 2.0 mmol/g sample, indicating an upper bound for effective amine deposition. It is noteworthy that all of these materials were made in duplicate and the TGA data is highly reproducible (See Appendix: Tables A.1-2).

Another interesting result is the anomalously low yield in going from the amine-SBA-15 to the G1 dendrimer. This low yield was attributed to the amines preferentially partitioning into the micropores and being subsequently unreactive due to inaccessibility of the larger cyanuric chloride and linker molecules. In an attempt to verify this hypothesis, a sample of SBA-15 was calcined at 900ºC to collapse the micropores and the G1 AMP-based hybrid was synthesized as described above. TGA performed on this sample showed a yield of 45% which is higher than the 35% yield for the sample with micropores (See Appendix: Table A.2).

3.3.4 Nitrogen Adsorption

The porosity of the dendrimer-SBA15 hybrid materials can be systematically controlled by increasing the dendrimer generation, dendrimer loading, and using three different linker molecules (P, AMP, TMDP). Nitrogen adsorption was used to quantify the porosity change as the dendrimer generation increases. Figure 3.7 shows the nitrogen adsorption isotherms for the first three generations of the AMP-based dendrimer hybrid. As shown in Figure 3.7, the relative pressure at which capillary condensation occurs shifts systematically to lower relative pressures as the dendrimer generation increases. This is consistent with the BJH analysis which shows a decrease of the effective mesopore diameter from 7.5, 6.7, to 5.2 nm for G1-AMP, G2-AMP, and G3-AMP, respectively (Table 3.2). Given the large organic content of these samples and the lack of a suitable reference material it should be emphasized that the pore sizes derived from the BJH analysis are subject to some error. That said clear trends are observed consistent with an increase of organic content in the SBA-15 mesopores; the trends are consistent with the TGA results. The pore volume also systematically decreases from 0.59, 0.41, to 0.20 cm^3 g^{-1} as the dendrimer generation increases from G1-AMP, G2-AMP, to G3-AMP, respectively (Table 3.2). These values are comparable to previous work [22]. These results indicate that a considerable fraction of dendrimers is formed in the mesopores and that the porosity can be controlled by changing the dendrimer generation.

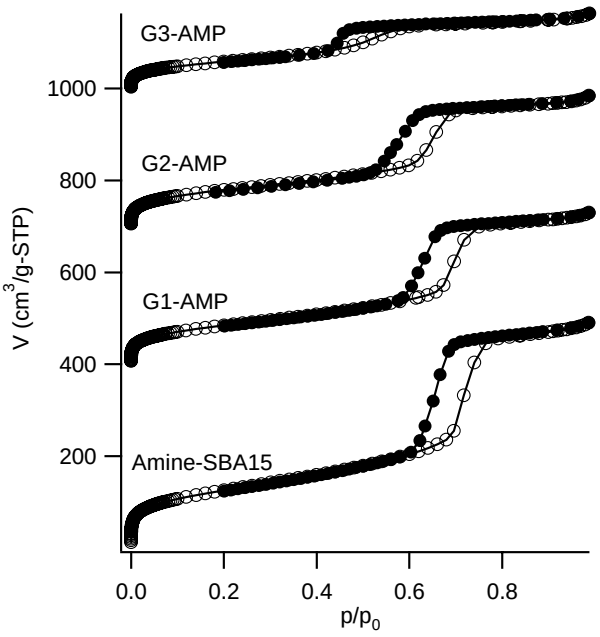

Figure 3.7 Adsorption isotherms illustrating the effect of generation on porosity. Adsorption branches are represented by unfilled circles, desorption branches by solid circles. The isotherms are shifted 400, 700, and 1000 cm^3/g-STP for G1-AMP, G2-AMP, and G3-AMP, respectively.

Table 3.2 Effect of dendrimer generation on hybrid porosity.

Sample ID	S(BET) [m^2/g]	S(α_s) [m^2/g]	V_{meso} [cm^3/g]	D_p(BJH) [nm]
0.5 mmol Amine	438	435	0.70	7.9
G2 P	302	307	0.43	7.0
G3 P	254	256	0.27	5.9
G1 AMP	429	414	0.59	7.5
G2 AMP	286	297	0.41	6.7
G3 AMP	193	205	0.20	5.2
G2 TMDP	220	228	0.31	6.7
G3 TMDP	194	200	0.19	5.2

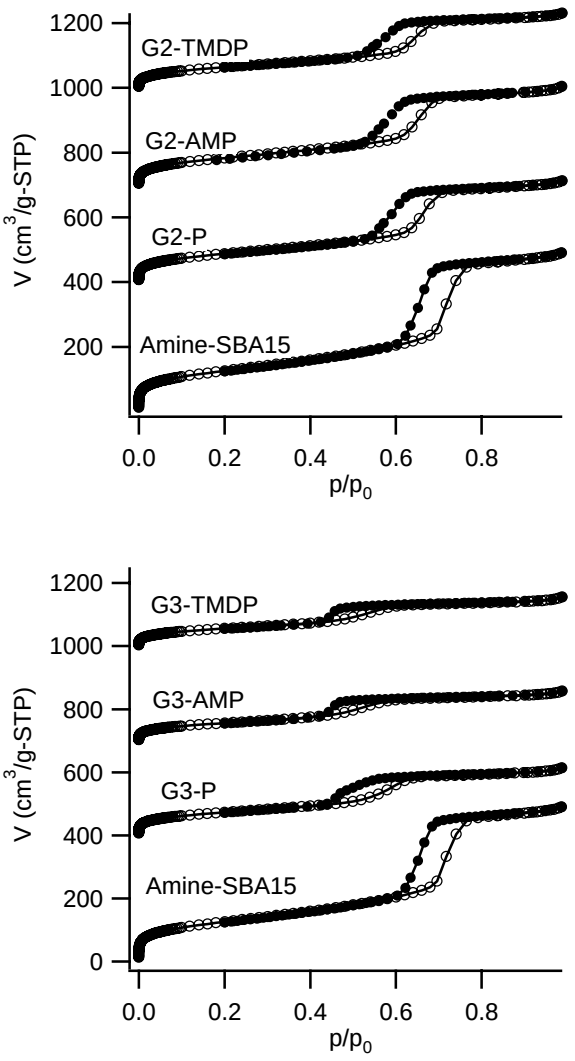

Figure 3.8 Adsorption isotherms illustrating the effect of different linkers on porosity. Adsorption branches are represented by unfilled circles, desorption branches by solid circles. The isotherms are shifted 400, 700, and 1000 cm^3/g-STP for P, AMP, and TMDP in 2nd and 3rd generation, respectively.

Table 3.3 Effect of different linkers on hybrid porosity.

Sample ID	S(BET) [m^2/g]	S(α_s) [m^2/g]	V_{meso} [cm^3/g]	D_p(BJH) [nm]
0.5 mmol Amine	438	435	0.70	7.9
G2 P	302	307	0.43	7.0
G2 AMP	286	297	0.41	6.7
G2 TMDP	220	228	0.29	6.7
G3 P	254	256	0.27	5.9
G3 AMP	193	205	0.20	5.2
G3 TMDP	194	200	0.19	5.2

The porosity of the hybrid materials can also be controlled using different linker molecules in the dendrimer synthesis. Figure 3.2 shows each linker molecule and their respective second-generation dendrimer. The linker sizes are P < AMP < TMDP, comparatively. Figure 3.8 shows the nitrogen-adsorption isotherms for the different dendrimers of various generation. A shift of the hysteresis loop to a lower pressure is observed as the size of linker molecule increases. Table 3.3 lists the pore size, surface area, and the adsorbed volume for hybrids with different linker molecules. The effective mesopore diameter, surface area, and the volume adsorbed decrease as the dendrimer size increases by changing the linker molecule from P to AMP. But both AMP and TMDP show similar values in the pore size, surface area, and the volume adsorbed in each generation. These similar values reflect the lower yields in the TMDP dendrimers as compared to AMP system, consistent with the TGA data in Table 3.3. The TMDP reacts less quantitatively than AMP offsetting the difference in size and resulting in similar organic contents. This difference in reactivity may be due to steric hindrance from other dendrimer groups. This result shows that the porosity can be controlled by altering the dendrimer size with different linker molecules.

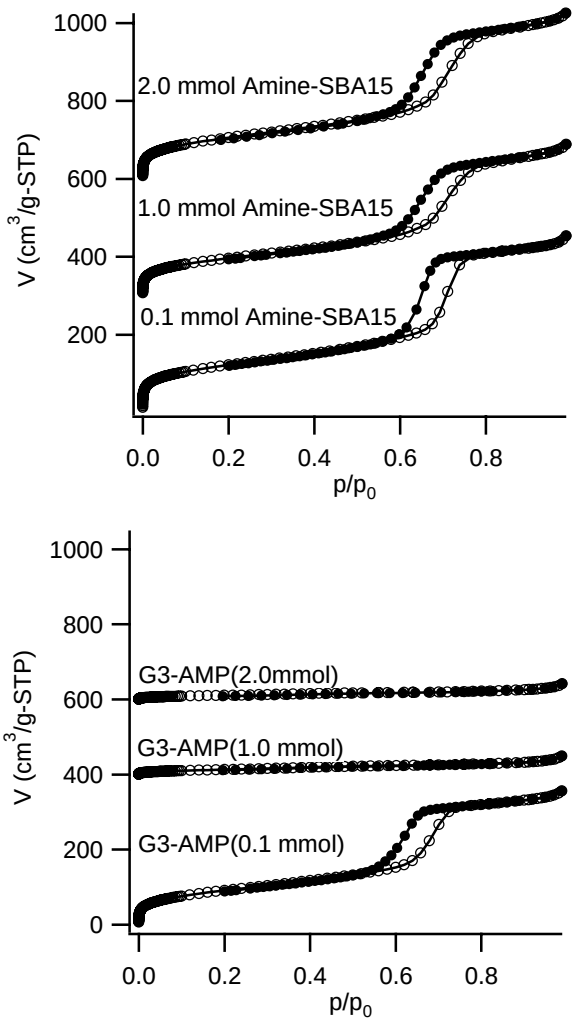

Figure 3.9 Adsorption isotherms illustrating the effect of the initial amine loading on porosity. Adsorption branches are represented by unfilled circles, desorption branches by solid circles. The isotherms are shifted 300 and 600 cm^3/g-STP for 1.0 mmol Amine-SBA-15 and 2.0 mmol Amine-SBA-15, respectively. And the isotherms are shifted 400 and 600 cm^3/g-STP for G3-AMP (1.0 mmol) and G3-AMP (2.0 mmol), respectively.

Table 3.4 Effect of initial amine loading on hybrid porosity.

Sample ID	S(BET) [m^2/g]	S(α_s) [m^2/g]	V_{meso} [cm^3/g]	D_p(BJH) [nm]
0.1 mmol Amine	430	416	0.57	8.3
1.0 mmol Amine	335	335	0.50	7.9
2.0 mmol Amine	367	368	0.55	7.9
G3 AMP (0.1 mmol)	315	322	0.46	7.5
G3 AMP (1.0 mmol)	43	53	~0	N/A
G3 AMP (2.0 mmol)	36	42	~0	N/A

The initial amine loading was varied from 0.1 mmol to 2.0 mmol per gram of SBA-15 to increase the organic content of the hybrids. Figure 3.9 shows the nitrogen-adsorption isotherms for the various initial amine loadings and its third generation AMP dendrimer. The isotherms indicate that the mesopores of SBA-15 are completely filled by the dendrimer for the samples with high initial amine loading. The G3-AMP with higher initial amine loadings (1.0 and 2.0 mmol) show a dramatic decrease in both the surface area and the volume adsorbed values compared to the samples with lower initial amine loadings (0.1 and 0.5 mmol). The samples prepared with high initial amine loadings (1.0 and 2.0 mmol) containing G3-dendrimers are essentially non-porous, in contrast to the samples with lower initial amine loadings: 0.45 and 0.20 cm^3/g for 0.1 and 0.5 mmol respectively (Table 3.4). This is also consistent with the TGA data that shows a substantial difference in organic content between the third generation hybrids grown on SBA-15 with high initial amine loadings (1.0 and 2.0 mmol per gram) compared with SBA-15 with low amine loadings (0.1 and 0.5 mmol per gram). This result shows that

the effective porosity can be modulated for a given dendrimer chemistry and oxide substrate by adjusting the dendrimer loading.

All results from adsorption experiments demonstrate that OMS/Dendrimer hybrids can be formed by the stepwise synthesis of melamine-based dendrimers that are grown directly off the mesopore surface. Further, the results indicate that the porosity of hybrids can be engineered by adjusting dendrimer generation, linker molecule, and the organic loading in a controllable way. The trends observed in the nitrogen adsorption data support this as the effective pore diameters, volumes, and surface areas decrease with: 1) increasing dendrimer generation for a fixed linker, 2) increasing the linker size for a fixed dendrimer generation, or 3) increasing the amine loading on the surface. The one exception to this is that AMP and TMDP show similar pore volumes and diameters even though TMDP is larger. TGA results indicate this is due to the TMDP being less reactive as the yields are lower for this linker as compared to AMP. Also, the high initial amine loading leads to a dramatic decrease in surface area and pore volume, which is correlated with the increase of organic content determined by TGA.

3.3.5 Copper(II) Sequestration

Copper(II) sequestration was used to demonstrate the accessibility of the peripheral primary amines and the increased separation potential of higher generation dendrimer hybrids. Evidence for recognition of Cu(II) by melamine-based dendrimers in solution has already been reported by Zhang and coworkers.[28] Here it is demonstrated this binding is still efficient when the dendrimers are tethered to a solid support. A 4-fold excess of cupric sulfate and a significant period of exposure (14 hours) were used in

order to determine the maximum sequestering potential of the dendrimer hybrids. The results of this experiment are shown in Figure 3.10. Comparing Figure 3.10 with Figure 3.6, which shows the organic content for these same samples, demonstrates the positive correlation between dendrimer size (i.e. number of peripheral and internal amines) and the maximum amount of copper that can be sequestered. As expected, SBA-15 proved to be a very poor copper scavenger taking up a negligible amount of copper, 0.01mmol/g. This result indicates that the copper uptake observed in the hybrids is not an artifact of copper binding to silanol groups. The amine-SBA-15 and dendrimer hybrids were able to sequester significant amounts of copper: 0.13 mmol/g, 0.35 mmol/g, 0.57 mmol/g, and 0.60 mmol/g for Amine-SBA-15 and the G1, G2, and G3 AMP-based hybrids, respectively.

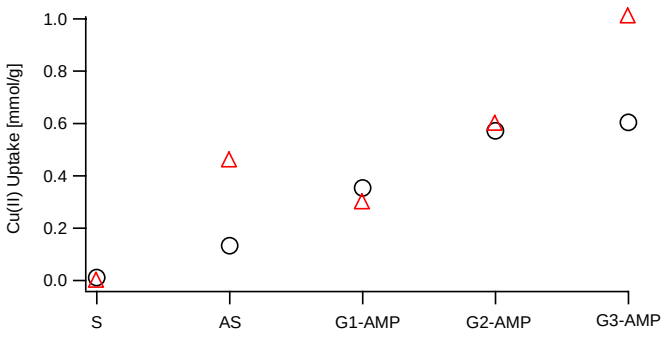

Figure 3.10 Copper(II) sequestration results. Data are shown for SBA-15 (S), 0.5mmol/g Amine-SBA-15 (AS), G1-AMP hybrid, G2-AMP hybrid, and G3-AMP hybrid: (Δ) maximum copper uptake assuming only Cu(II)-N_2O_2 and Cu(II)-N_4 complexes form; (O) actual values.

Ottaviani and coworkers reported that their PAMAM dendrimers formed Cu(II)-N_2O_2 and Cu(II)-N_4 complexes upon the addition of Cu(II).[69,70] The Cu(II)-N_2O_2 complex forms with two peripheral primary amines and two water molecules; the Cu(II)-N_4 complex forms with two peripheral amines and two internal tertiary amines. In our melamine-based dendrimers the Cu(II)-N_2O_2 complex should likewise form with the peripheral amines and water. It could also be argued that the Cu(II)-N_4 complex should form between the two tertiary amines which are found at the branching point on adjacent AMP molecules and the two following amines on the same AMP molecules which include the secondary amines within the dendrimer framework and the primary amines on the periphery.

Assuming that these two complexes are the only ones that form in substantial quantities, the maximum uptake for each sample can be estimated from TGA data: 0.00 mmol/g (SBA-15), 0.46 mmol/g (Amine-SBA-15), 0.30 mmol/g (G1-AMP), 0.60 mmol/g (G2-AMP), and 1.01 mmol/g (G3-AMP). The G1 and G2 dendrimer hybrids deviate by only ±0.05 mmol/g from these predicted values. The Amine-SBA-15 and G3 hybrid deviate from the predicted values by more than 0.30 mmol/g. The small amount of copper sequestered using the Amine-SBA-15 sample seems to add support to the view that a large portion of the amines are located in the micropores and remain inaccessible. One possible explanation for the G3 hybrid's performance is that the increased density in the dendrimer's outer shell prevents copper from binding to the amines within the dendrimer framework. Assuming that copper can only bind to the peripheral amines for the G3-AMP hybrid, the maximum copper uptake would be 0.58 mmol/g which is only 0.02 mmol/g lower than the observed quantity.

3.4 Summary and Conclusions

Dendrimer/SBA-15 hybrids are synthesized and characterized using several analytical techniques. The hybrid porosity can be systematically altered by varying 1) the dendrimer generation, 2) the linker molecule, and 3) the surface amine loading. Given the accessibility demonstrated by Cu(II) sequestration the materials have accessible functional groups that can be used for catalysis, separations, molecular recognition, or as scaffolds to build more complex structures. Ongoing work is optimizing the synthesis conditions for higher dendrimer yields, and our results suggest the presence of micropores has a deleterious effect on dendrimer yield.

CHAPTER IV

APPLICATIONS IN ENANTIOSELECTIVE CATALYSIS AND CONCLUDING REMARKS

4.1 Introduction

The last chapter demonstrates the ability to tune the pore size, volume and surface area of melamine-based dendrimer/SBA-15 hybrids, and their ability to sequester metals such as copper (II). The next step is to show their usefulness as a catalyst support. Our motivations for the development of a L-proline/OMS hybrid using melamine-based dendrimers as an organic scaffold are threefold: 1) attaching a homogeneous catalyst to a solid support makes it easy to remove, recover and reuse; 2) heterogeneous organocatalysis is an environmentally friendly approach because there are no metal centers; and 3) the development of an effective enantioselective heterogeneous catalyst reduces industrial separation costs.

Simultaneously and as preparation for the heterogeneous catalysis, it seems appropriate to prepare L-proline derivatives of dendrimers in solution. This will be done for several reasons: 1) these solution-based analogs will help us better understand how to tune properties on a solid support; 2) the building blocks for these "full" dendrimers will be prepared in the process of synthesizing the convergently prepared dendrimer hybrids as will be shown below; 3) dendrimers are easier to characterize by NMR & mass spectroscopy in solution; and 4) these systems are interesting in and of themselves and may prove to be more useful than the heterogeneous catalysts in some applications. The

rest of this chapter will deal with the preliminary work performed in these two areas and what will be done in the future.

4.2 Preliminary Work

Three L-proline derivatives have been synthesized, two of which had their catalytic activity qualitatively analyzed for a test reaction and compared with L-proline. These compounds are shown in Figure 4.1 and their syntheses are shown in Figures 4.2 and 4.3 for **A** and **B**, **C**, respectively. The purpose of these syntheses was to obtain some basic understanding of how the catalytic properties of L-proline are affected when attached to simple dendrimer-like structures and attached to SBA-15.

4.2.1 Material Syntheses

Derivative **A** was synthesized using a "one pot" approach (Figure 4.2). 0.1 mmol CC was reacted at room temperature with 0.1 mmol N-Boc-cis-4-amino-L-proline methyl ester hydrochloride salt (CAP) in 2 mL DCM using 0.22 mmol DIPEA as a proton mop. After approximately one hour, 0.1 mmol of *m*-(trifluoromethyl)benzaldehyde and 0.11 mmol DIPEA was added. After ~24 hours, 0.1 mmol Piperidine and 0.11 mmol DIPEA was added to the reaction mixture. This step took several days to reach completion. Each step was monitored using TLC and Mass Spectroscopy. The product was subsequently purified using silica gel chromatography and then deprotected in two steps using concentrated HCl to remove the Boc group and then concentrated NaOH to deesterify the carboxylic acid.

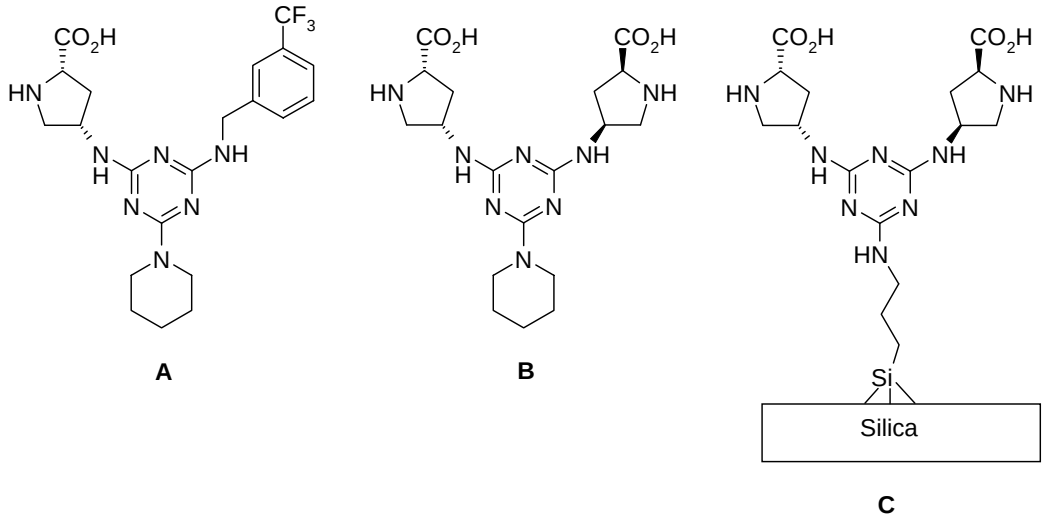

Figure 4.1 Structures of the L-proline-triazine derivatives synthesized.

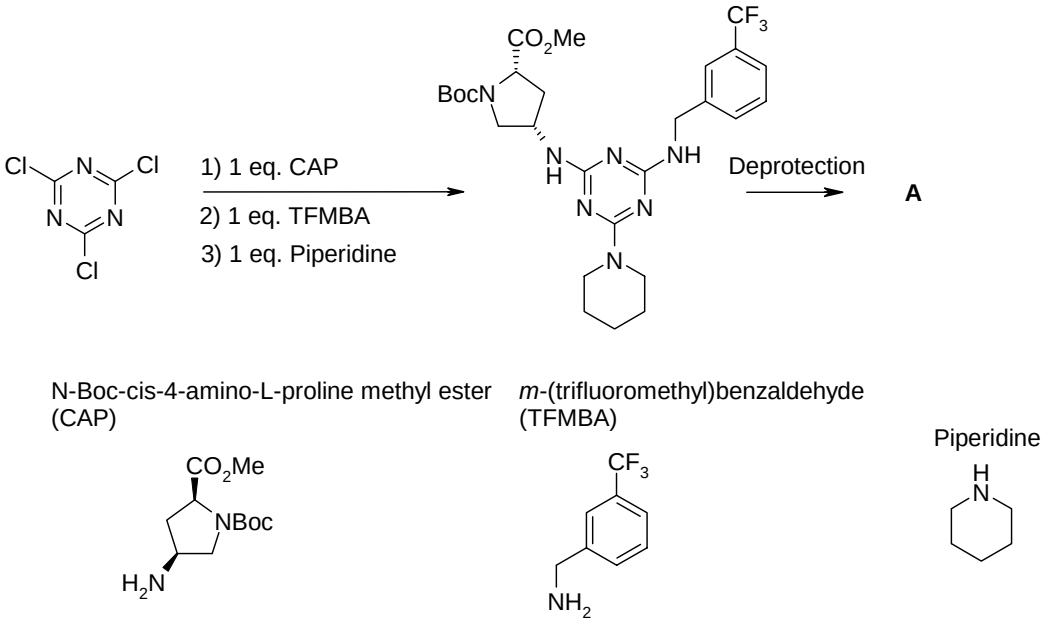

Figure 4.2 The synthesis of derivative **A**.

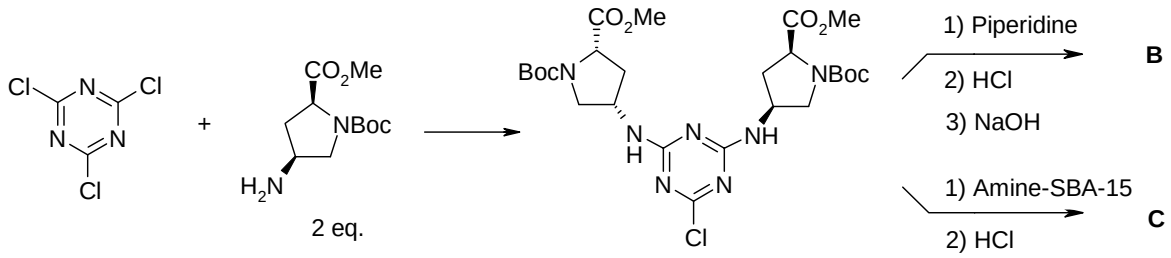

Figure 4.3 The syntheses of derivatives **B** and **C**.

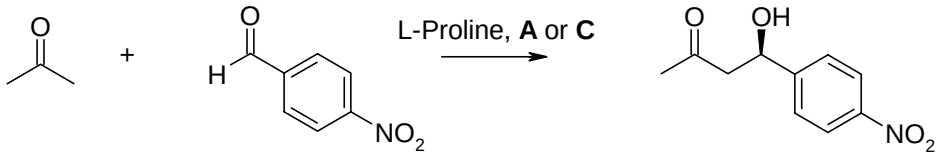

Figure 4.4 The aldol reaction used to test the catalytic activities of **A** and **C**.

Derivatives **B** and **C** were synthesized simultaneously (Figure 4.3). 0.6 mmol CAP were reacted with 0.3 mmol CC in 3 mL DCM and 3.3 mmol DIPEA. After ~24 hours, one mL of this mixture was removed and reacted with 1 equivalent 0.5 mmol/g Amine-SBA-15 for ~24 hours. 0.2 mmol Piperidine was added to the remaining mixtureand after ~ 24 hours purified using silica gel chromatography. Concentrated HCl was added to both products to remove the protecting groups. Concentrated NaOH was subsequently added to **B** but was not used on derivative **C** to avoid dissolving the silica structure.

4.2.2 Catalytic Analysis and Results

L-proline and derivative **A** and **C** were tested separately for their catalytic activity in the aldol reaction of *p*-nitrobenzaldehyde with acetone (Figure 4.4). This reaction was chosen because it has been extensively studied by List and others.[46,52-54] ~0.03 mmol of each catalyst were added to 1 mL of 4:1 DMSO/Acetone and stirred for 20 minutes. 0.1 mmol *p*-nitrobenzaldehyde was then added and reacted for ~24 hours. Neither L-proline or A were very soluble in the DMSO/Acetone mixture.

The color of the reaction mixture using L-proline turned a dark orange brown. The reaction mixture using **A**, similarly, turned orange. The mixture using **C** showed no color change. TLC showed multiple products were produced for the reactions catalyzed with L-proline and **A**, however, **A** produced a smaller number of products than L-proline. **C** showed no observable activity. Each of these reaction mixtures were extracted into ethyl acetate and analyzed using chiral chromatography. Many product peaks appeared for L-proline, a few for **A** and no observable peaks for **C**. However, on these first few

runs, the resolution was poor, the peak intensities were low and the residence times were over an hour for some compounds.

4.2.3 Conclusions

There is work which needs to be done in order to completely analyze the three catalysts **A**, **B** and **C** and their products. TLC indicates that catalyst **A** is catalytically active toward some of the many products L-proline produces, indicating that **A** is more selective than L-proline. However, whether any of these are the desired aldol is not known as of yet; the products need to purified and characterized. Based on this result **B** should prove to be active in this same sense, though it has yet to be tested. **C** should also be active because it is attached to the same branching group as **A** and should behave similarly.

There are, however, several issues that may have contributed to **C**'s poor performance. First, in each of the other catalyst preparations, HCl was unable to fully remove the methyl group from the protected carboxylic acid in spite of heating and long durations of exposure. As noted above, NaOH was used for the others, but due to silica stability issues was not used on **C**. Second, a higher concentration of the di-L-proline monochlorotriazine and a longer reaction probably needs to be used in order to cap all the primary amines on the surface. And lastly, it has not been satisfactorily characterized. These issues withstanding, the preliminary work shows promise for L-proline functionalized dendrimers and dendrimer hybrids. The rest of this chapter will be devoted to future work building off of this preliminary work.

4.3 Future Work

4.3.1 L-proline Derivatized Dendrimer Hybrids

There are two aspects of L-proline silica hybrids on which upcoming research will be focused: 1) Is L-proline catalytically active when attached to silica using melamine-based dendrimers as an organic scaffold? 2) How does the dendrimer generation and surface chemistry influence that activity?

The first question will be obtained by resolving the above issues with catalyst **C**. I need to determine whether or not the di-L-proline monochlorotriazine was attached to the silica surface. This can be done by employing two methods: TGA and FTIR. TGA will tell us approximately how much organic has been added and FTIR will be able to tell us whether it has actually been covalently attached to the amine-functionalized surface or just physisorbed. If it was successfully attached to the surface with a relatively high yield, it needs to be determined whether the protected carboxylic acid was deesterified. Removal of the Boc group occurs within a few minutes of adding concentrated HCl. FTIR should also be able to tell us if there are esters present. If HCl was not successful, a better deprotection method or synthesis route needs to be developed in order to ensure a the active sites of the L-proline are deprotected.

Once this has been done, higher generation L-proline derivatized dendrimers using piperizine will be attached/grown on the surface using both convergent and divergent dendrimer synthesis approaches. The divergent approach was described in Chapter III. The convergent synthesis will proceed as shown in Figure 4.5. If a successfully synthesized catalyst **C** does not show activity, this will provide a way to observe whether activity is dependant upon the loading. If **C** does show activity, this will

demonstrate how the increased loading affects the *ee* and yield. This set of syntheses will be repeated employing a β-alanine spacer (Figure 4.6) between L-proline and the dendrimer which will give it more flexibility and cause it to more closely imitate homogeneous catalysis.

Finally, the effects of modifiying the surface of the silica will be investigated (Figure 4.7). Many reports have shown that interactions with surface silanols has a detrimental effect on *ee*. This study will include both polar and nonpolar surface modifiers such as amines and alkyl chains.

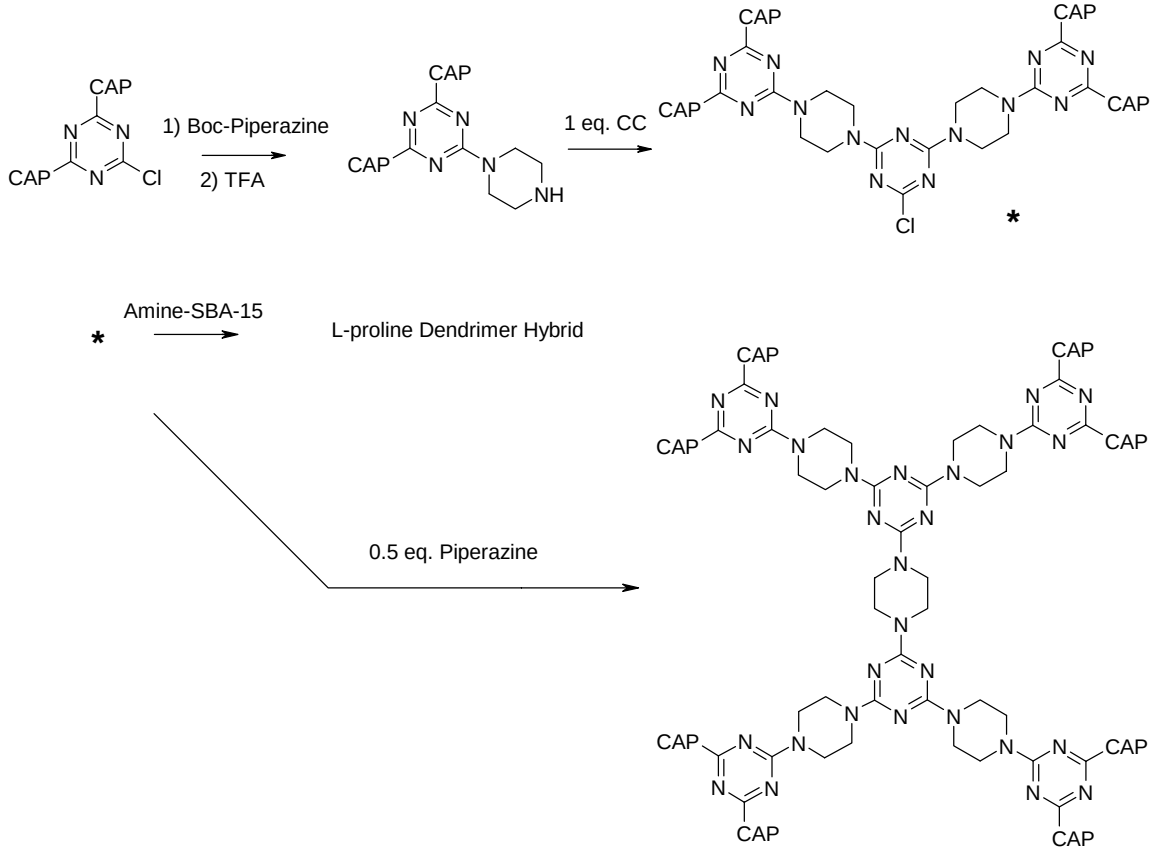

Figure 4.5 Convergent construction of dendrons and dendrimer hybrids.

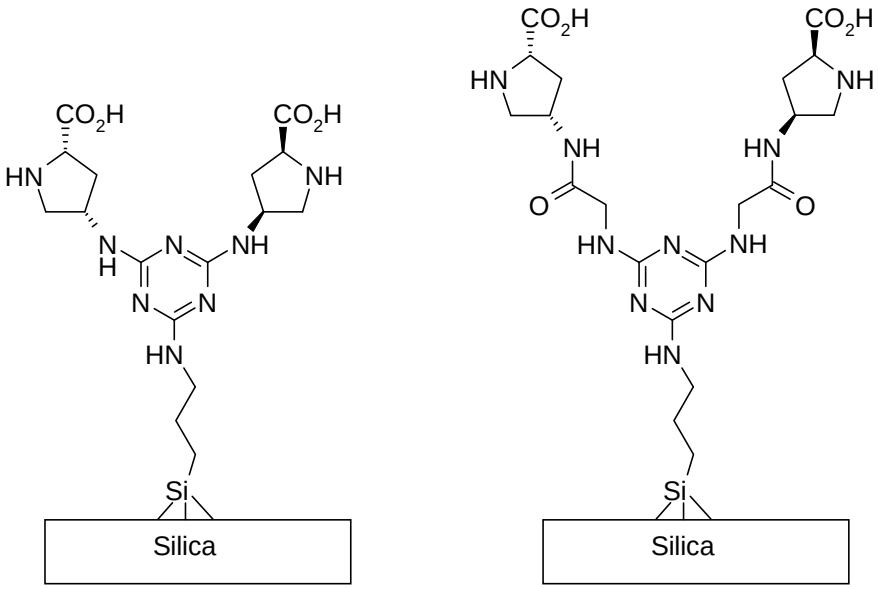

Figure 4.6 L-Proline catalysts with and without a β-alanine linker.

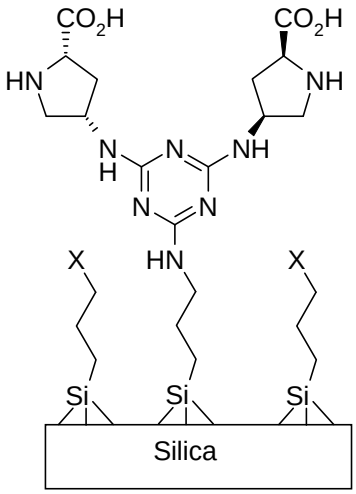

Figure 4.7 Surface modification of silica. X will be varied between both polar and nonpolar functional groups.

4.3.2 L-Proline Derivatized Dendrons

As mentioned above and shown in Figure 4.5, for every convergently prepared hybrid, "full" dendrimers will be prepared. When reacting monochlorotriazine (*****) with a primary amine on the silica surface, a large excess needs to be used. Piperazine can be added to the unreacted monochlorotriazine to form dendrimers. The catalytic properties of L-proline on dendrimers will be compared with those of their respective hybrids.

As noted above in the Material Syntheses section, neither L-proline nor the dendrimer derivatives are very soluble in DMSO and Acetone. Investigations concerning the way to increase the solubility will be performed. This may include changing the organic spacer (β-alanine) to something more hydrophilic or alternating L-proline and a more soluble compound on the dendrimer periphery.

REFERENCES

(1) Rouquerol, F.; Rouquerol, J.; Sing, K. *Adsorption by Powders and Porous Solids*; Academic: San Diego, 1999.

(2) Barrer, R. M. *Zeolites and Clay Materials as Sorbents and Molecular Sieves*; Academic: London, 1978.

(3) Alfredsson, V.; Anderson, M. W. *Chem. Mater.* **1996**, *8*, 1141-1146.

(4) Beck, J. S.; Vartuli, J. C.; Roth, W. J.; Leonowicz, M. E.; Kresge, C. T.; Schmitt, K. D.; Chu, C. T. W.; Olson, D. H.; Sheppard, E. W.; McCullen, S. B.; Higgins, J. B.; Schlenker, J. L. *J. Am. Chem. Soc.* **1992**, *114*, 10834-10843.

(5) Kresge, C. T.; Leonowicz, M. E.; Roth, W. J.; Vartuli, J. C.; Beck, J. S. *Nature* **1992**, *359*, 710-712.

(6) Zhao, D. Y.; Huo, Q. S.; Feng, J. L.; Chmelka, B. F.; Stucky, G. D. *Journal of the American Chemical Society* **1998**, *120*, 6024-6036.

(7) Zhao, D. Y.; Feng, J. L.; Huo, Q. S.; Melosh, N.; Fredrickson, G. H.; Chmelka, B. F.; Stucky, G. D. *Science* **1998**, *279*, 548-552.

(8) Kleitz, F.; Choi, S. H.; Ryoo, R. *Chem. Commun.* **2003**, *17*, 2136-2137.

(9) Corma, A. *Chem. Rev.* **1997**, *97*, 2373-2419.

(10) Ford, D. M.; Simanek, E. E.; Shantz, D. F. *Nanotechnology* **2005**, *16*, S458-S475.

(11) Moller, K.; Bein, T. *Chem. Mater.* **1998**, *10*, 2950-2963.

(12) Sanchez, C.; Ribot, F. *New Journal of Chemistry* **1994**, *18*, 1007.

(13) Lim, M. H.; Stein, A. *Chem. Mater.* **1999**, *11*, 3285-3295.

(14) Burkett, S. L.; Sims, S. D.; Mann, S. *Chem. Commun.* **1996**, 1367-1368.

(15) Fowler, C. E.; Burkett, S. L.; Mann, S. *Chem. Commun.* **1997**, 1769-1770.

(16) McKittrick, M. W.; Jones, C. W. *Chem. Mater.* **2003**, *15*, 1132-1139.

(17) Defaud, V.; Davis, M. E. *J. Am. Chem. Soc.* **2003**, *125*, 9403-9413.

(18) Huh, S.; Wiench, J. W.; Yoo, J.-C.; Pruski, M.; Lin, V. S. Y. *Chem. Mater.* **2003**, *15*, 4247-4256.

(19) Huh, S.; Wiench, J. W.; Yoo, J.-C.; Pruski, M.; Lin, V. S. Y. *Chem. Mater.* **2003**, *15*, 2364-2365.

(20) Huh, S.; Chen, H.-T.; Wiench, J. W.; Pruski, M.; Lin, V. S. Y. *J. Am. Chem. Soc.* **2004**, *126*, 1010-1011.

(21) Reynhardt, J. P. K.; Yang, Y.; Sayari, A.; Alper, H. *Chem. Mater.* **2004**, *16*, 4095-4102.

(22) Acosta, E. J.; Carr, C. S.; Simanek, E. E.; Shantz, D. F. *Advanced Materials* **2004**, *16*, 985-+.

(23) Tomalia, D. A.; Naylor, A. M.; Goddard, W. A. *Angew. Chem. Int. Ed.* **1990**, *29*, 138-175.

(24) Simanek, E. E.; Gonzalez, S. O. *J. Chem. Ed.* **2002**, *79*, 1222-1231.

(25) Hawker, C. J.; Frechet, J. M. J. *Chem. Commun.* **1990**, 1010.

(26) Zhang, W.; Simanek, E. E. *Org. Lett.* **2000**, *2*, 843-845.

(27) Acosta, E. J.; Gonzalez, S. O.; Simanek, E. E. *J. Poly. Sci. A* **2005**, *43*, 168-177.

(28) Zhang, W.; Simanek, E. E. *Tetrahedron Letters* **2001**, *42*, 5355-5357.

(29) Zhang, W.; Nowlan, D. T. I.; Thomson, L. M.; Lackowski, W. M.; Simanek, E. E. *J. Am. Chem. Soc.* **2001**, *123*, 8914-8922.

(30) Zhang, W.; Tichey, S. E.; Perez, L. M.; Maria, G.; Lindahl, P. A.; Simanek, E. E. *J. Am. Chem. Soc.* **2003**, *125*, 5086-5094.

(31) Tuel, Z. *Zeolites* **1995**, *15*, 236-242.

(32) Ulgappan, N.; Krishnasamy, U. *J. Chem. Soc., Chem. Commun.* **1995**, 373-374.

(33) Serrano, D. P.; Li, H. X.; Davis, M. E. *J. Chem. Soc., Chem. Commun.* **1992**, 745-747.

(34) Tuel, A.; Ben-Taarit, Y. *J. Chem. Soc., Chem. Commun.* **1994**, 1667-1676.

(35) Reddy, K. M. *Catal. Lett.* **1994**, *23*, 175-187.

(36) Camblor, M. A.; Corma, A.; Perez-Pariente, J. *Zeolites* **1993**, *13*, 82-87.

(37) Wight, A. P.; Davis, M. E. *Chem. Rev.* **2002**, *102*, 3589-3614.

(38) Song, C. E.; Lee, S.-G. *Chem. Rev.* **2002**, *102*, 3495-3524.

(39) Fan, Q.-H.; Li, Y.-M.; Chan, A. S. C. *Chem. Rev.* **2002**, *102*, 3589-3614.

(40) McMurry, J. *Organic Chemistry*; 5 ed.; Brooks/Cole: Pacific Grove, 2000.

(41) Kirby, A. J. *Angew. Chem. Int. Ed.* **1996**, *35*, 770-790.

(42) Murakami, Y.; Kikuchi, J.; Hisaeda, Y.; Hayashida, O. *Chem. Rev.* **1996**, *96*, 721-758.

(43) Wulff, G. *Chem. Rev.* **2002**, *102*, 1-28.

(44) Eder, U.; Sauer, G.; Wiechert, R. *Angew. Chem. Int. Ed.* **1971**, *10*, 496-497.

(45) Hajos, Z. G., D. R. Parrish *J. Org. Chem* **1974**, *39*, 1615.

(46) List, B.; Lerner, R. A.; Barbas III, C. F. *J. Am. Chem. Soc.* **2000**, *122*, 2395-2396.

(47) List, B. *J. Am. Chem. Soc.* **2000**, *122*, 9336-9337.

(48) List, B.; Pojarliev, P.; Biller, W. T.; Martin, H. J. *Tetrahedron* **2002**, *124*, 827-833.

(49) List, B. *J. Am. Chem. Soc.* **2002**, *124*, 5656-5657.

(50) List, B. *Acc. Chem. Res.* **2004**, *37*, 548-557.

(51) List, B.; Hoang, L.; Martin, H. J. Proceedings of the National Academy of Sciences, 2004; p 5839-5842.

(52) Mase, N.; Tanaka, F.; Barbas III, C. F. *Org. Lett.* **2003**, *5*, 4369-4372.

(53) Mase, N.; Tanaka, F.; Barbas III, C. F. *Angew. Chem. Int. Ed.* **2004**, *43*, 2420-2423.

(54) Notz, W.; Sakthivel, K.; Bui, T.; Zhong, G.; Barbas III, C. F. *Tetrahedron Lett.* **2001**, *42*, 199-201.

(55) Notz, W.; Tanaka, F.; Barbas III, C. F. *Acc. Chem. Res.* **2004**, *37*, 580-591.

(56) Bahmanyar, S.; Houk, K. N. *J. Am. Chem. Soc.* **2001**, *123*, 9922-9923.

(57) Bahmanyar, S.; Houk, K. N. *J. Am. Chem. Soc.* **2001**, *1123*, 11273-11283.

(58) Rajagapol, D.; Moni, M. S.; Subramanian, S.; Swaminathan, S. *Tetrahedron Asymmetry* **1999**, *10*, 1631-1634.

(59) Dhar, D.; Beadham, I.; Chandrasekaran, S. *Proc. Indian Acad. Sci. (Chem. Sci.)* **2003**, *115*, 365-372.

(60) Bengalia, M.; Cinquini, M.; Cozzi, F.; Puglisi, A.; Celentano, G. *Adv. Synth. Catal.* **2002**, *344*, 533-542.

(61) Bengalia, M.; Puglisi, A.; Cozzi, F. *Chem. Rev.* **2003**, *103*, 3401-3429.

(62) Ladd, M. F. C.; Palmer, R. A. *Structure Determination by X-ray Crystallography*; Plenum: New York, 1977.

(63) Carr, C. S. "Design and Control of Hiearchically Structured Nanomaterials," Texas A&M University, 2005.

(64) Barrett, E. P.; Joyner, L. G.; Halenda, P. P. *J. Am. Chem. Soc.* **1951**, *73*, 373-380.

(65) Kruk, M.; Jaroniec, M.; Sayari, A. *Langmuir* **1997**, *13*, 6267-6273.

(66) Beesley, T. E.; Scott, R. P. W. *Chiral Chromatography*; John Wiley & Sons: Chichester, 1998.

(67) Szejtli *Chem. Rev.* **1998**, *98*, 1743-1753.

(68) Gregg, S. J.; Sing, K. S. W. *Adsorption, Surface Area, and Porosity*; Academic Press: London, 1982.

(69) Ottaviani, M. F. *J. Phys. Chem. B* **1997**, *101*, 158-166.

(70) Ottaviani, M. F.; Turro, N. J.; Jockbush, S.; Tomalia, D. A. *J. Phys. Chem. B* **2003**, *107*, 2046-2053.

APPENDIX

Table A.1 Effect of the dendrimer modification on the porosity of Dendrimer/SBA-15 hybrids.

(A)

Sample ID	S(BET) [m^2/g]	S(alpha-s) [m^2/g]	V_{meso} [cm^3/g]	Dp(BJH) [nm]
0.5 mmol Amine	438	435	0.70	7.9
G2 P	299	301	0.41	7.0
G3 P	248	251	0.27	5.9
G1 AMP	291	296	0.46	7.4
G2 AMP	275	276	0.37	6.7
G3 AMP	201	214	0.20	5.2
G2 TMDP	274	285	0.38	6.7
G3 TMDP	213	221	0.21	5.2

(B)

Sample ID	S(BET) [m^2/g]	S(alpha-s) [m^2/g]	V_{meso} [cm^3/g]	Dp(BJH) [nm]
0.1 mmol Amine	533	550	0.83	7.9
0.5 mmol Amine	438	435	0.70	7.9
2.0 mmol Amine	336	340	0.56	7.9
G3 AMP (0.1 mmol)	298	306	0.42	7.0
G3 AMP (0.5 mmol)	201	214	0.20	5.2
G3 AMP (1.0 mmol)	19	20	0	0
G3 AMP (2.0 mmol)	14	17	0	0

Table A.2 TGA data: (A) Dendrimer size effects; (B) Amine loading effects; (C) Micropore effects

(A)

Sample ID	Organic [wt%]	Organic [mmol/g SBA-15]	Step Yield
0.5 mmol Amine	5%	0.97	-----
G2 P	17%	0.22	-----
G3 P	28%	0.215	93%
G1 AMP	11%	0.34	31%
G2 AMP	19%	0.25	73%
G3 AMP	29%	0.19	76%
G2 TMDP	20%	0.24	-----
G3 TMDP	30%	0.28	116%

(B)

Sample ID	Organic [wt%]	Organic [mmol/g SBA-15]
0.1 mmol Amine	2%	0.31
G3 AMP (0.1 mmol)	14%	0.07
1.0 mmol Amine	6%	1.12
G3 AMP (1.0 mmol)	37%	0.27
2.0 mmol Amine	6%	1.06
G3 AMP (2.0 mmol)	38%	0.28

(C)

Sample ID	Organic [wt%]	Organic [mmol/g SBA-15]	Step Yield
0.5 mmol Amine	5%	0.97	-----
G1 AMP	11%	0.34	31%
0.5 mmol Amine (No Micropores)	2%	0.43	-----
G1 AMP (No Micropores)	7%	0.20	45%

VITA

Jonathan David Lunn received his Bachelor of Science degree in chemical engineering from Texas A&M University in May 2004. He entered the chemical engineering graduate program at Texas A&M University in September of the same year and received his Master of Science degree in May 2006. He is currently working on his PhD in the same department. Mr. Lunn may be reached at Texas A&M University, TAMU 3122, College Station, TX 77840. His email address is jdlunn@tamu.edu.